Aerosol transmittance for clear-sky solar irradiance models: Review and validation of an accurate universal parameterization

AUTHOR'S MANUSCRIPT VERSION

Published in RSER (doi:10.1016/j.rser.2021.111061)

José A. Ruiz-Arias[a,*]

[a]*Applied Physics I, University of Málaga, Málaga, Spain.*

ARTICLE INFO

Keywords:
aerosol transmittance
universal
parameterization
clear-sky solar radiation

ABSTRACT

Accurate modeling of solar radiation under cloudless situations is important to facilitate the development and exploitation of the renewable solar resource worldwide. However, many existing clear-sky solar radiation models perform inconsistently under varying aerosol conditions. This work presents a worldwide review of some of the most widely known clear-sky solar radiation models and shows that most of these inconsistencies are related to deficiencies in the simulation of the extinction by aerosols. As a remedy, a fast yet highly accurate analytical parameterization of the aerosol transmittance is introduced here. A performance evaluation using worldwide ground observations of aerosol Ångström's parameters has shown that, conversely to the existing parameterizations, the new one performs consistently under all possible aerosol conditions with virtually no bias and no dispersion. At seven arid locations, in particular, it is found that, when the new aerosol parameterization is used, the direct normal irradiance (DNI) predictions of the reviewed clear-sky irradiance models are comparable to those made with the high-performance RRTMG physical model. This fact proves that the deficiencies in the simulation of aerosol extinction produce most of the DNI biases of clear-sky solar irradiance models in arid regions. Thus, the performance differences found in such models in previous benchmarking studies can vanish by using a better parameterization of the aerosol transmittance such as the one proposed here.

1. Introduction

Solar energy production peaks during cloudless situations, hence the regions with the greatest solar resource have low prevalence of clouds. Consequently, accurate modeling of solar radiation under these situations is important to ease the development and exploitation of the renewable solar resource worldwide. Moreover, an accurate evaluation of solar radiation under hypothetical cloudless situations—for which clear-sky solar radiation models are specifically devised [1, 2, 3, 4]—is of utmost importance for multiple applications such as the evaluation of all-sky solar irradiance from satellite imagery [5, 3], evaluation of photovoltaics performance [6], cloud screening [7], synthetic high-frequency solar irradiance data generation [8], cloud type classification [9] or the separation of global solar irradiance into its direct and diffuse components [10]. In all these tasks, the selection of a proper clear-sky solar radiation model is crucial and must be done carefully since it may constraint the prediction accuracy and the simulated performance of solar energy systems. However, many existing clear-sky solar radiation models have been found to perform inconsistently in two

*Corresponding author
jararias@uma.es (J.A. Ruiz-Arias)
ORCID(s): 0000-0003-4220-1751 (J.A. Ruiz-Arias)

recent comprehensive benchmarking studies [3, 11], that confirm previous ones [2, 12]. These model inconsistencies are often related to the use of oversimplified parameterizations of the extinction by aerosols, such as neglecting the spectral dependence of aerosol optical depth [1], and likely combined with potential over-fittings. The reasons for a high level of simplification in these models are described in what follows.

In general, the assessment of surface solar radiation using computational models is an essential aspect in nearly all the development phases of solar energy projects, from their inception through their exploitation, and at multiple scales, from local to regional. Although solar radiation is fundamentally spectral, many of these solar energy applications only require the total broadband solar irradiance. Thus, a conventional approach to reduce the computational burden consists in using broadband approximations to avoid demanding spectral calculations. This approach has been found successful for both cloudless skies [13, 14, 15, 16, 17, 18, 1, 2, 12, 3] and cloudy atmospheres [19, 20, 21, 22].

A common approach to circumvent the spectral calculations considers independent broadband parameterizations of the solar irradiance transmittances for each atmospheric constituent, from which solar irradiance is subsequently evaluated. For instance, the most straightforward and widely used approach to evaluate the broadband direct normal irradiance (DNI), E_{bn}, from broadband transmittances is:

$$E_{bn} = E_{on}\ \varepsilon\ T_R\ T_g\ T_o\ T_w\ T_a \tag{1}$$

where E_{on} is the broadband extraterrestrial solar irradiance at normal incidence and mean Sun-Earth distance, ε is the Sun-Earth's distance correction factor and T_k are the independent broadband transmittances for Rayleigh scattering (R), absorption by uniformly-mixed gases (g), ozone (o) and water vapor (w), and extinction by aerosols (a).

The broadband transmittance T_k for the atmospheric constituent k is most typically defined as a weighted average of the spectral transmittance, $T_{k\lambda}$, for the constituent k, as follows:

$$T_k = \frac{\int_{\Delta\lambda} E_{0n\lambda}(\lambda)\ T_{k\lambda}(\lambda)\ d\lambda}{\int_{\Delta\lambda} E_{0n\lambda}(\lambda)\ d\lambda}, \tag{2}$$

where λ is the wavelength, $\Delta\lambda$ is the spectral integration interval and $E_{0n\lambda}$ is the extraterrestrial solar radiation spectrum at normal incidence and mean Sun-Earth distance. Since $E_{0n\lambda}$ does not have an analytical rendering, any functional representation of Eq. (2) appears utopian regardless of the functional form of $T_{k\lambda}$. Hence, in practice, Eq. (2) is parameterized by custom wavelength-independent functional forms with parameters empirically adjusted. For instance, the BIRD model [13] evaluates Eq. (2) for water vapor as $\left(1 - 2.4959u_w\right) / \left[(1 + 79.034u_w)^{0.6828} + 6.385u_w\right]$, where $u_w = m\,w$, with m being the air mass and w the total-column water vapor content, usually referred to as precipitable water. This general approach reduces the computational burden involved in Eq. (2) by two orders of magnitude, or

more, but as with any empirical fit, may suffer from locality issues and lack of generality.

Direct normal irradiance, defined as in Eq. (1), assumes that light extinction processes are *independent* from each other at broadband level. However, this is strictly true only for monochromatic radiation in diluted media [23]. In parallel, Eq. (2) simplifies the parameterization of broadband transmittances to facilitate the development of numerical parameterizations. Such simplification is used by most clear-sky solar modelers, and for that reason is considered here. This approach is preferred to alternate definitions that are known to be exact but greatly entangle the parameterization of T_k [24]. A detailed discussion on the definition of broadband transmittance and its implications is out of the scope of this work. The interested reader is referred to the seminal papers of Molineaux and Ineichen [24] and Gueymard [25] on this topic, or to a more recent and brief description in Ref. [4].

Of interest in the present context, however, is the relative error associated with the combined use of Eq. (1) and Eq. (2). A simple inspection of Fig. 1 and Fig. 2 in [24] reveals that, when considering all atmospheric constituents together, the expected error's magnitude in broadband transmittance is generally negligible but can be as high as ≈5 % when the air mass exceeds ≈2.

1.1. Broadband aerosol transmittance

Among all the extinction processes that solar photons undergo in a cloudless atmosphere, extinction by aerosols is potentially the most important one. As a reference, for an overhead sun (*i.e.,* solar zenith angle of 0°), the broadband transmittance by the uniform mixture of gases in the atmosphere is ≈0.9, and remains fairly stable within the range of typical ground surface elevations. In parallel, the broadband transmittance by atmospheric water vapor stays typically within the interval 0.8–0.9 for the range of precipitable water amounts normally found on earth. (See Ref. [26] for more details about the range of variation of this and other transmittances.) In contrast, the variation of broadband transmittance by aerosols is much greater. It may drop to values of only 0.4 in hazy environments, such as during desert sandstorms or in heavily polluted areas, and can also change widely on a daily basis [27]. Atmospheric aerosol constitute an important source of inter-model discrepancies [12, 2], which can limit the modeling accuracy [28]. This reveals that a thorough modeling of broadband aerosol transmittance is required to guarantee a correct model performance under every potential atmospheric situation. To that effect, an accurate parameterization of Eq. (2) for atmospheric aerosols is needed, namely:

$$T_a = \frac{\int_{\Delta\lambda} E_{0n\lambda}(\lambda)\, T_{a\lambda}(\lambda)\, d\lambda}{\int_{\Delta\lambda} E_{0n\lambda}(\lambda)\, d\lambda}, \tag{3}$$

where T_a and $T_{a\lambda}$ are the broadband and spectral aerosol transmittances, respectively. In virtue of Bouguer's law [29], the spectral aerosol transmittance is evaluated as:

$$T_{a\lambda}(\lambda) = e^{-m_a \tau_{a\lambda}(\lambda)}, \tag{4}$$

where m_a is the aerosol optical air mass [30] and $\tau_{a\lambda}$ is the spectral aerosol optical depth (AOD), which, in virtue of Ångström's law [31], is evaluated as:

$$\tau_{a\lambda}(\lambda) = \beta \left(\frac{\lambda}{\lambda_0} \right)^{-\alpha}, \tag{5}$$

where $\lambda_0 = 1$ μm, β is AOD at 1 μm, customarily known as Ångström turbidity coefficient, and α is the Ångström wavelength exponent. The latter is related to the aerosol particle size distribution and modulates the spectral variation of $\tau_{a\lambda}$. Roughly speaking, low values of α (below $\approx$1) are associated with a prevalence of coarse particles, (typically, dust or sea salt), while α values above $\approx$1.5 indicate prevailing fine particles, typically associated with pollution or smoke from biomass burning.

Compared with the parameterization of extinction by other atmospheric constituents, the parameterization of broadband aerosol transmittance (Eq. 3) is particularly challenging, not only because of the much wider range of potential variation of T_a but also because of the important variations in spectral AOD, which may lead to remarkably different broadband solar radiation extinctions even in situations with apparently similar AOD. In this sense, Fig. 1 shows the spectral aerosol transmittance for relatively clean and very turbid atmospheric conditions combined with dusty, rural or polluted environments. The different size distributions of aerosol particles change the AOD spectral response and produce variations in the spectral extinction from extremely high extinction in the ultraviolet region to very little in the infrared. At the broadband level, these spectral changes can have a significant impact. For instance, for $\beta = 0.1$, T_a increases from 0.68 to 0.85 when α decreases from 2.3 to 0.3. This result highlights the importance of considering α in the parameterization of T_a to ensure the global-scale validity of such parameterization, despite it introduces modeling difficulties. For instance, the convoluted spectral dependence of AOD apparently led the authors of the MRMv6 model [32] to avoiding the computational burden reduction of the parameterized approach. Instead, they perform an explicit spectral integration of Eq. (3), with the consequence that using MRMv6 in demanding large-scale applications, such as the evaluation of gridded solar radiation from satellite imagery [5, 33], would probably be impractical if not impossible.

This work reviews the parameterization of Eq. (3) for broadband aerosol transmittance in some classical and recent clear-sky solar radiation models (hereinafter referred to as CSR models). It is shown in Section 2 that all these models

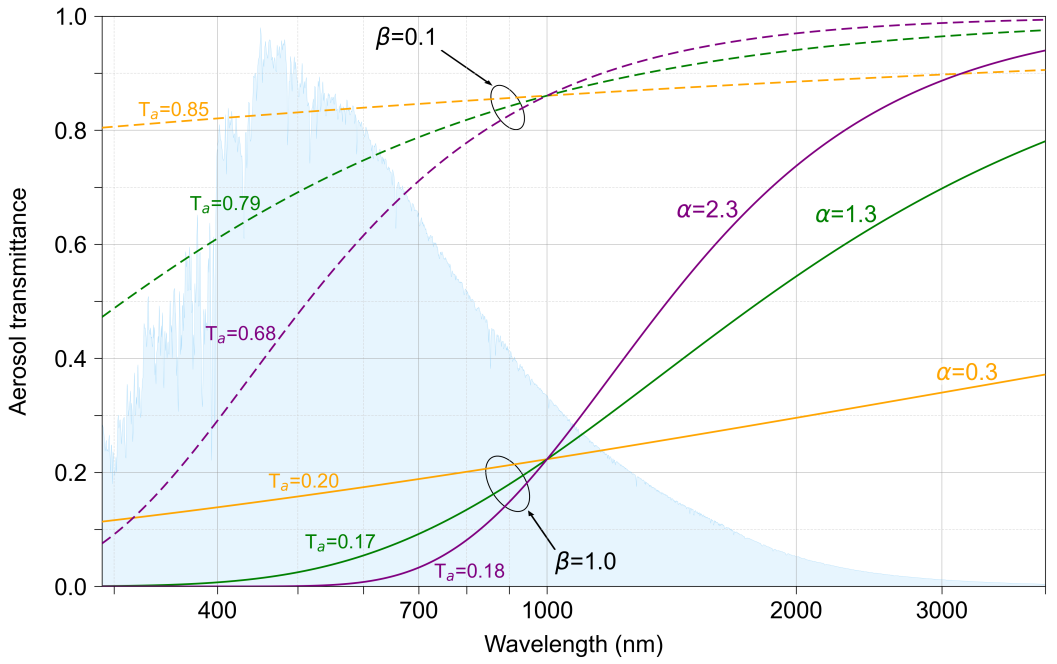

Figure 1: Spectral aerosol transmittance computed according to Eqs. (4–5) for two values of Angström turbidity coefficient (0.1 for clean conditions, and 1.0 for extremely turbid conditions), as well as three values of Angström wavelength exponent (0.3 for dusty, 1.3 for rural and 2.3 for polluted environments). All cases assume $m_a = 1.5$. The plot also shows the Gueymard [34] extraterrestrial solar radiation spectrum in the background to note that the wavelengths in the visible region receive the highest weights at computing T_a.

present shortcomings that prevent their use under challenging aerosol conditions, often including land areas with the greatest solar resource. As a remedy, a novel fully analytical and universal parameterization of the broadband aerosol transmittance is proposed in Section 3. It is verified in Section 4, using global distributions of AOD from a ground observing network, and further used in Section 5 in combination with existing CSR models to largely improve their DNI estimates as compared against a research-class observational dataset at arid locations. Section 6 summarizes the main conclusions of the study.

The code used to conduct this research, and to create most figures included in the paper, is provided freely in the supplementary material, together with additional extended figures.

2. Review of existing aerosol transmittance parameterizations

A major motivation here is to improve the parameterization of Eq. (2) in combination with Eq. (1) to accurately evaluate E_{bn}. As the literature on this topic suggests, the use of this pair of equations entails two potential sources of error: *(a)* the *approximation error* associated with the simplifications in both Eq. (1) and Eq. (2), and *(b)* the potential *numerical error* associated with the numerical parameterization of Eq. (2). The approximation error is tolerated to

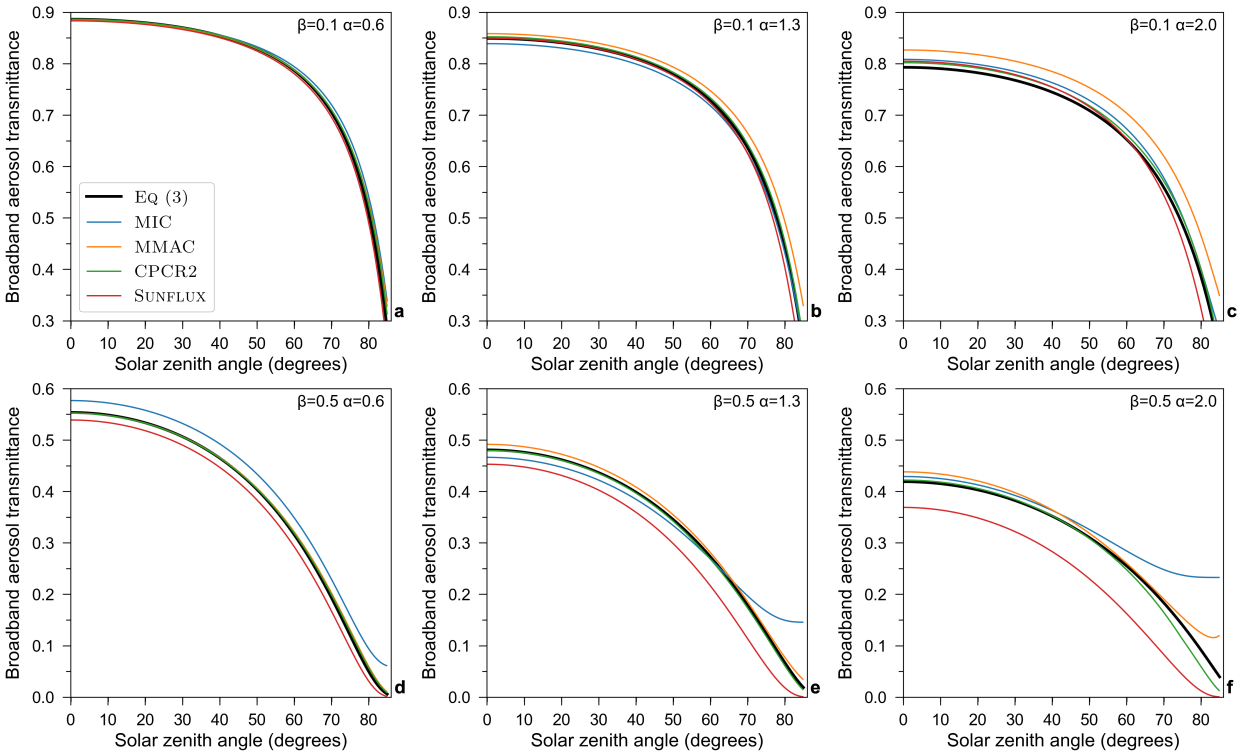

Figure 2: Broadband aerosol transmittance as directly evaluated by Eq. (3) and by the aerosol parameterizations in the MIC, MMAC, CPCR2 and SUNFLUX models, for various combinations of β and α values, as a function of solar zenith angle.

keep the solar radiation model simple and tractable. But then an accurate parameterization of Eq. (2) is required to keep the total error low. This is particularly relevant to aerosols because the errors in the parameterization of their transmittance can be of the same magnitude or even greater than the approximation error *(a)*.

For illustration purposes, Figs. 2 and 3 compare the T_a parameterized values for a selection of well-known CSR models against the ones computed directly from Eq. (3), which is used as a reference here because it eliminates the numerical error *(b)*, although it is based on the simplifying assumption that the aerosol layer is located at the top of the atmosphere and is thus directly illuminated by the extraterrestrial solar spectrum. The comparison is made for clean (upper row) and hazy (lower row) situations combined with dusty (left column), rural (middle column) and polluted (right column) conditions. All aerosol parameterizations are presented in Appendix A, where the reader is referred to for a thorough description of the actual numerical parameterizations reviewed here. Eq. (3) is computed using the Gueymard [34] extraterrestrial solar irradiance spectrum between 290 and 4000 nm.

Figure 2 shows the results for the aerosol transmittance parameterizations used in the MIC, MMAC, CPCR2 and SUNFLUX models. All of them account for the impact of the spectral AOD variability using the Ångström α parameter or, as in the case of SUNFLUX, using the spectral AOD values at 550 and 870 nm. In general, the models stay closer to

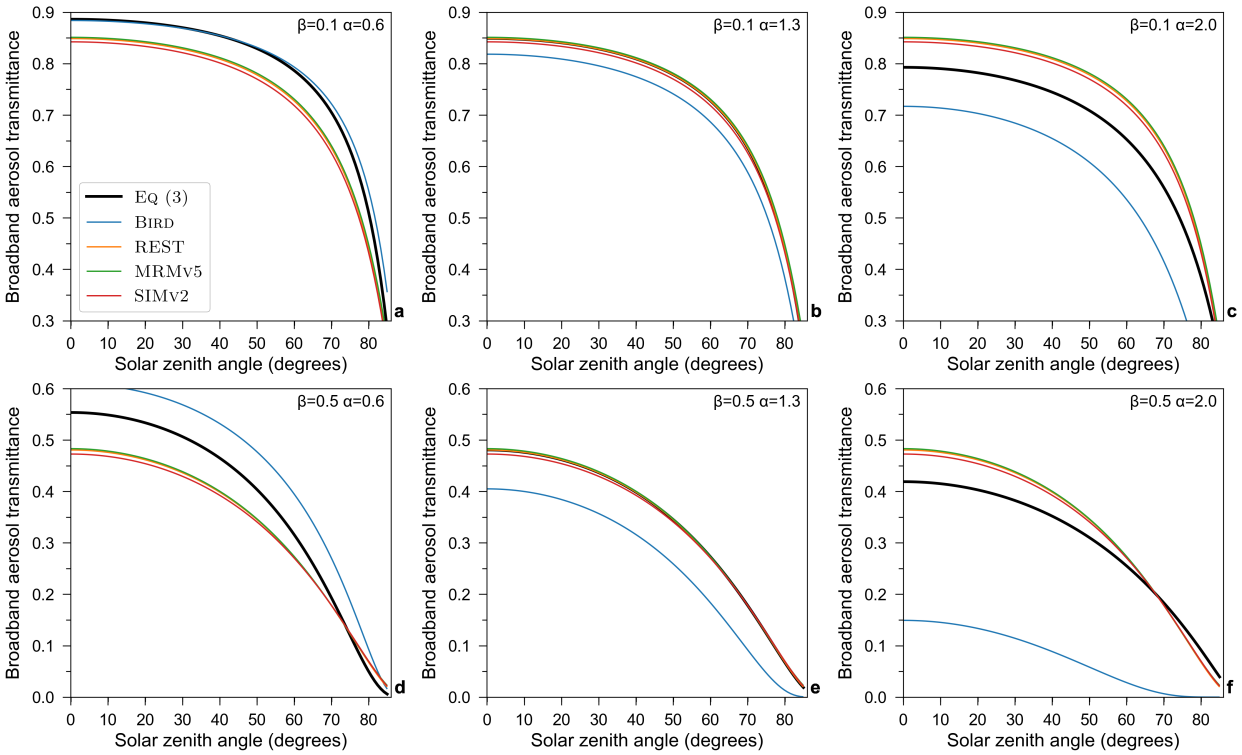

Figure 3: Same as Fig. 2 but for the BIRD, REST, MRMv5 and SIMv2 models. The calculation for MRMv5 assumes sea-level pressure.

Eq. (3) under the assumed clean atmosphere than under hazy conditions. SUNFLUX and MIC are relatively consistent regardless of the value of α in the clean atmosphere (upper row of panels) but their performance degrades as the atmosphere becomes hazier (lower row of panels) and α is larger. This is especially true in the case of SUNFLUX, which might indicate that, to parameterize T_a, the use of two monochromatic AODs is less effective than the explicit use of α. The MIC model largely overestimates T_a at large solar zenith angles, which confirms the findings reported in [2]. CPCR2 performs very consistently, with low deviations for all situations, except for large α. In that situation, it slightly overestimates Eq. (3) for low β and low solar zenith angles, and underestimates it for high β and high solar zenith angles. MMAC keeps close to Eq. (3) for low α but overestimates it when α increases. Overall, there is no model that consistently remains close to Eq. (3) no matter the cleanliness, haziness, aerosol size distribution or solar position, which constitutes a caveat to the universality assumption of such models. For instance, from Fig. 2, MMAC provides good estimates of T_a in dusty environments (high β, low α) but fails under polluted conditions (high β, high α).

Figure 3 shows the results for the aerosol transmittance parameterizations used in the BIRD, REST, MRMv5 and SIMv2 models. All of them disregard the use of α to parameterize T_a and only rely on β. BIRD is the one exception.

As SUNFLUX, it uses two spectral AOD values, but at 380 and 500 nm. However, these values are deemed so close each other that probably cannot represent properly the spectral trend of AOD. The results in Fig. 3 are very illustrative of the shortcomings when the spectral AOD dependence is neglected. All the models, except BIRD, which performs nearly as an outlier, provide a virtually perfect fit to Eq. (3) for rural conditions, i.e., $\alpha = 1.3$. However, they fail resoundingly as soon as the atmosphere turns dusty or polluted, which, in practice, discourage the use of such models for a large portion of worldwide land areas, in particular, some of the areas with the greatest solar resource.

3. Description of the new aerosol transmittance parameterization

Starting with Eq. (3), and performing a Taylor expansion of Eq. (4) in the spectral band $\Delta\lambda$ around its central wavelength, $\bar{\lambda}$, it is found that the total aerosol transmittance throughout $\Delta\lambda$ can be evaluated as:

$$T_a = T_{a\lambda}(\bar{\lambda}) \sum_{n=0}^{\infty} I_n P_n(\phi), \tag{6}$$

where

$$I_n = \frac{1}{n!} \int_{\Delta\lambda} \left(\frac{\lambda}{\bar{\lambda}} - 1 \right)^n \left[\frac{E_{0n\lambda}(\lambda)}{\int_{\Delta\lambda} E_{0n\lambda}(\lambda)} \right] d\lambda \tag{7}$$

are coefficients that only depend on $E_{0n\lambda}$ and $P_n(\phi)$ are n-order recursive polynomials of the variable $\phi = m_a \, \alpha \, \tau_{a\lambda}(\bar{\lambda})$ that are defined as:

$$P_n(\phi) = \begin{cases} 1, & \text{if } n = 0 \\ \phi \sum_{i=1}^{n} A_{n,i} P_{n-i}(\phi), & \text{if } n \geq 1 \end{cases} \tag{8}$$

where

$$A_{n,i} = (-1)^{i+1} \frac{\prod_{j=1}^{n} (\alpha + j)}{\prod_{j=i}^{n} (\alpha + j)} c_{n,i}, \tag{9}$$

$c_{n,1} = c_{n,n} = 1$ and $c_{n,i} = c_{n-1,i-1} + c_{n-1,i}$. A detailed derivation of Eqs. (6–9) is presented in Appendix B.

The parameterization described by Eq. (6) evaluates the aerosol transmittance throughout the spectral band $\Delta\lambda$ by means of the spectral aerosol transmittance at its center, $T_{a\lambda}(\bar{\lambda})$, corrected with a multiplicative factor given by the sum of an infinite series. Each term of the series is the product of a coefficient I_n, which conveys information on the solar radiation spectrum within $\Delta\lambda$, and a polynomial $P_n(\phi)$, which conveys information regarding solar position (i.e., m_a)

and atmospheric turbidity (i.e., β and α). Note that, in practice, the coefficients I_n only must be computed once for each selection of spectral bands and that this calculation does not involve any numerical fit.

Since the parameterization is based on a Taylor expansion, its performance is expected to degrade as the width of the spectral band around $\bar{\lambda}$ increases. To prevent this, the band can be divided in M smaller disjoint sub-bands of width $\Delta\lambda_j$ to which the parameterization is applied independently to compute each sub-band transmittance $T_{a,j}$. The total broadband transmittance is then obtained as:

$$T_a = \sum_{j=1}^{M} f_j \, T_{a,j}, \tag{10}$$

where

$$f_j = \frac{\int_{\Delta\lambda_j} E_{0n\lambda}(\lambda) d\lambda}{\int_{\Delta\lambda} E_{0n\lambda}(\lambda) d\lambda} \tag{11}$$

and $\sum_{j=1}^{M} f_j = 1$. This multiband approach is used in advanced physical radiative transfer models [35] and some CSR models [14, 16, 36].

In practice, the infinite series in Eq. (6) must be truncated to a finite number N of terms that retain the accuracy required in every intended application. Hence, some tradeoff exists between the number M of spectral sub-bands and the number N of terms retained in the sum of the infinite series. The latter is hereinafter referred to as *order of approximation*, or simply, *order*, such that the 0-th order of approximation (N=0) only considers the first term of the infinite series, the 1-st order of approximation (N=1) considers the first two terms, the 2-nd order (N=2) considers the first three terms, and so on.

4. Performance analysis

This section describes various aspects of the performance of the parameterization described in Section 3. To that aim, the integrals in Eq. (3) are solved numerically for each triplet (m_a, β, α) using the trapezoidal integration rule [37] and the extraterrestrial solar radiation spectrum for the spectral range 290–4000 nm Gueymard [34], which describes the mean solar spectral irradiance (in W m^{-2} nm^{-1}) at normal incidence and mean Sun-Earth distance in steps of 0.5 nm between 290 and 400 nm, 1 nm between 400 and 1705 nm, and 5 nm between 1705 and 4000 nm. The results of this integration process are used as benchmark references to measure the performance of the parameterization. The new aerosol parameterization will be hereinafter referred to as TAYLOR-N, where N={0, 1, 2...} is the order of approximation.

Table 1
Waveband I_n coefficients for each spectral band considered in this study and parameterization orders of approximation from 0 to 3. They have been computed from Eq. (7) using the extraterrestrial solar irradiance spectrum in the range from 290 to 4000 nm [34].

N	Broadband	UVVIS	IR	NIR	SIR
0	1.0	1.0	1.0	1.0	1.0
1	−0.57722	0.03822	−0.46533	−0.09371	−0.23905
2	0.20095	0.02321	0.13797	0.02430	0.04930
3	−0.04597	0.00069	−0.02623	−0.00127	−0.00541

Table 2
Mean wavelength and broadband fraction (Eq. 11) for each spectral band considered in this study. They have been computed from the extraterrestrial solar irradiance spectrum in the range 290–4000 nm [34].

	Broadband	UVVIS	IR	NIR	SIR
$\bar{\lambda}$ (nm)	2145	495	2350	1100	2750
f_j	1.0	0.4708	0.5292	0.4038	0.1254

4.1. Order of approximation and number of sub-bands

Figure 4 compares the predictions of the Taylor parameterization with order of approximation increasing from 0 to 3 combined with the following spectral splitting choices spanning the range from 290 through 4000 nm:

- One single band: 290–4000 nm, in Figs. 4a–c.

- Two sub-bands: ultraviolet and visible regions combined (UVVIS, 290–700 nm) and infrared region (IR, 700–4000 nm), in Figs. 4d–f.

- Three sub-bands: UVVIS, near IR (700–1500 nm, NIR) and short IR (1500–4000 nm, SIR), in Figs. 4g–i.

The polynomials $P_n(\phi)$ up to third order are as follows:

$$P_0(\phi) = 1 \tag{12a}$$

$$P_1(\phi) = \phi \tag{12b}$$

$$P_2(\phi) = \phi\,[\phi - (\alpha + 1)] \tag{12c}$$

$$P_3(\phi) = \phi\left[\phi^2 - 3(\alpha + 1)\phi + (\alpha + 1)(\alpha + 2)\right]. \tag{12d}$$

The coefficients I_n up to the third order of approximation and for each spectral sub-band considered here are provided in Table 1. The mean wavelength and broadband fraction of each spectral band are indicated in Table 2.

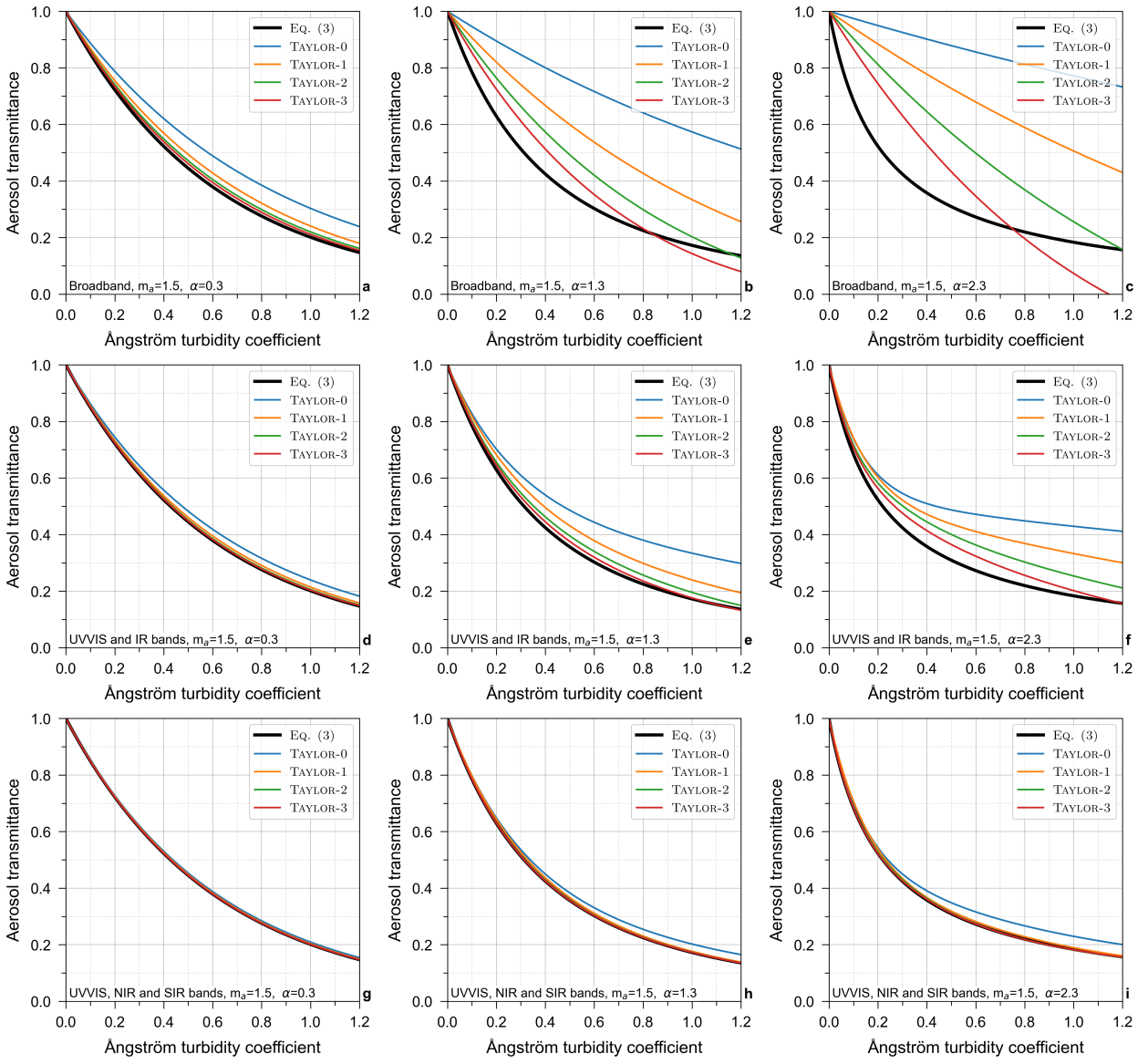

Figure 4: Comparison of the reference broadband aerosol transmittance and the Taylor parameterization for the combination of various orders of approximation (0, 1, 2 and 3), the three sub-band divisions of the solar spectral range described at the beginning of Section 4 (top to bottom) and three values of α (0.3, 1.3 and 2.3; left to right). A fixed value of 1.5 is assumed for m_a.

A general overview of Fig. 4 shows that, relatively to Eq. (3), the Taylor parameterization error grows with increasing α values (i.e., from left to right panels) since an increase in α results in a steeper variation of T_a for low β values. Similarly, decreasing the width of the spectral sub-bands, or equivalently, increasing the number of them, (i.e., from top to bottom panels) improves the Taylor approximation and, subsequently, the parameterization's performance.

More specifically, when $\alpha = 0.3$ and only one single band is considered (Fig. 4a), only the 2-nd and 3-rd orders of

Table 3
Mean absolute deviation (MAD), i.e., mean of the absolute deviations, between the reference broadband aerosol transmittance (Eq. 3) and the Taylor parameterization for orders of approximation from 0 to 3 combined with the spectral sub-band divisions shown in Fig. 4 and three values of α (0.3, 1.3 and 2.3). The value of m_a is assumed fixed to 1.5. Values smaller than 0.01 are highlighted in bold face.

	$\alpha = 0.3$			$\alpha = 1.3$			$\alpha = 2.3$		
# bands	1	2	3	1	2	3	1	2	3
TAYLOR-0	0.090	0.033	**0.007**	0.349	0.122	0.025	0.515	0.176	0.037
TAYLOR-1	0.039	0.013	**0.003**	0.186	0.063	**0.008**	0.347	0.120	0.010
TAYLOR-2	0.020	**0.005**	**0.000**	0.088	0.028	**0.001**	0.181	0.071	**0.003**
TAYLOR-3	0.012	**0.002**	**0.000**	0.052	0.012	**0.000**	0.122	0.035	**0.001**

Table 4
As Table 3 but for $m_a = 6$ (80° solar zenith angle).

	$\alpha = 0.3$			$\alpha = 1.3$			$\alpha = 2.3$		
# bands	1	2	3	1	2	3	1	2	3
TAYLOR-0	0.043	0.017	**0.004**	0.223	0.103	0.019	0.432	0.206	0.033
TAYLOR-1	0.014	**0.005**	**0.001**	0.097	0.034	**0.003**	0.186	0.071	**0.004**
TAYLOR-2	**0.007**	**0.002**	**0.000**	0.071	0.022	**0.001**	0.246	0.069	**0.002**
TAYLOR-3	**0.004**	**0.001**	**0.000**	0.045	0.012	**0.000**	0.221	0.065	**0.001**

approximation (TAYLOR-2 and TAYLOR-3, respectively) are able to follow the variation of the reference T_a given by Eq. (3), although with non-negligible deviations. More specifically, the mean absolute deviation (MAD) is 0.020 for TAYLOR-2 and 0.012 for TAYLOR-3 (see Table 3). As α increases, the performance of the models degrades sharply, making necessary to increase the number of sub-bands (Fig. 4b–c).

Using two sub-bands (UVVIS and IR, Figs. 4d–f) provides a large improvement over the single-band results. In particular, the TAYLOR-2 and TAYLOR-3 approximations agree closely with the reference T_a when $\alpha = 0.3$ (MAD values of 0.005 and 0.002, respectively), but they still overestimate more or less significantly for greater α values. They would not be appropriate if, for instance, 0.01 was proposed as an upper tolerance limit for MAD. For further reference, values smaller than 0.01 are highlighted in bold face in Table 3.

When three spectral sub-bands are considered (Figs. 4g–i)—specifically, UVVIS, NIR and SIR—virtually any approximation order provides a good estimate of the reference T_a for $\alpha = 0.3$, while linear or higher orders of approximation provide good estimates for greater α values. In general, both TAYLOR-2 and TAYLOR-3 combined with the three-band division of the solar spectral range provide the best results regardless of α.

When greater aerosol optical air masses are considered, the 2-nd and higher orders of approximation become fluctuating for large α values when they are combined with either the one-band or two-band scenario. However, when

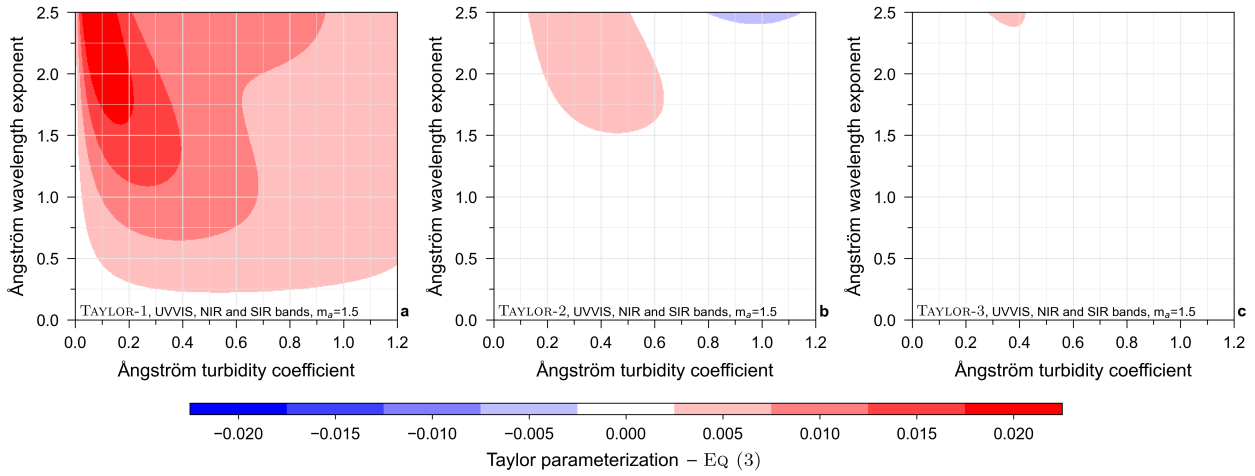

Figure 5: Difference between the 3-band Taylor parameterization and the reference T_a in the space (β, α). The Taylor parameterization has orders of approximation 1 (panel a), 2 (panel b), and 3 (panel c). The solar spectral range is divided in the UVVIS, NIR and SIR bands. A fixed value $m_a = 1.5$ is assumed.

they are combined with the three-band division, they show even better performance than for lower values of m_a, as shown in Table 4. These results suggest that the 2-nd or 3-rd approximation orders should be used in combination with the 3-band division of the solar spectral range.

4.2. Parameterization performance with three spectral sub-bands

Following with the results obtained in the previous section, this section delves into the performance of the Taylor parameterization combined with the division of the solar spectrum into three spectral sub-bands, namely, UVVIS, NIR and SIR.

Figure 5 shows the difference in the (β, α) space between the TAYLOR-1, TAYLOR-2 and TAYLOR-3 parameterizations and the reference T_a from Eq. (3), assuming m_a fixed to 1.5 and the 3-band division (UVVIS, NIR and SIR). The Ångström turbidity coefficient runs from 0 through 1.2 and Ångström wavelength exponent runs from 0 through 2.5 to cover most situations that can be expected anywhere, regardless of the aerosol regime. TAYLOR-2 and TAYLOR-3 provide deviations below 0.0075, in magnitude, for any Ångström turbidity coefficient or wavelength exponent. More specifically, the TAYLOR-2 deviations are below 0.0025, in magnitude, for most of the (β, α) space, and, virtually, in all that space with TAYLOR-3. This means that TAYLOR-3 is a near perfect match for the direct integration of Eq. (3) under extreme circumstances, such as desert dust storms, smoke episodes, or strong pollution events in rural or continental environments.

Figure 6 shows the same results as Fig. 5, but in the (β, m_a) space, so that the performance of the Taylor parameterization is now evaluated against solar position. Since, according to Fig. 5, the greatest deviations occur for large

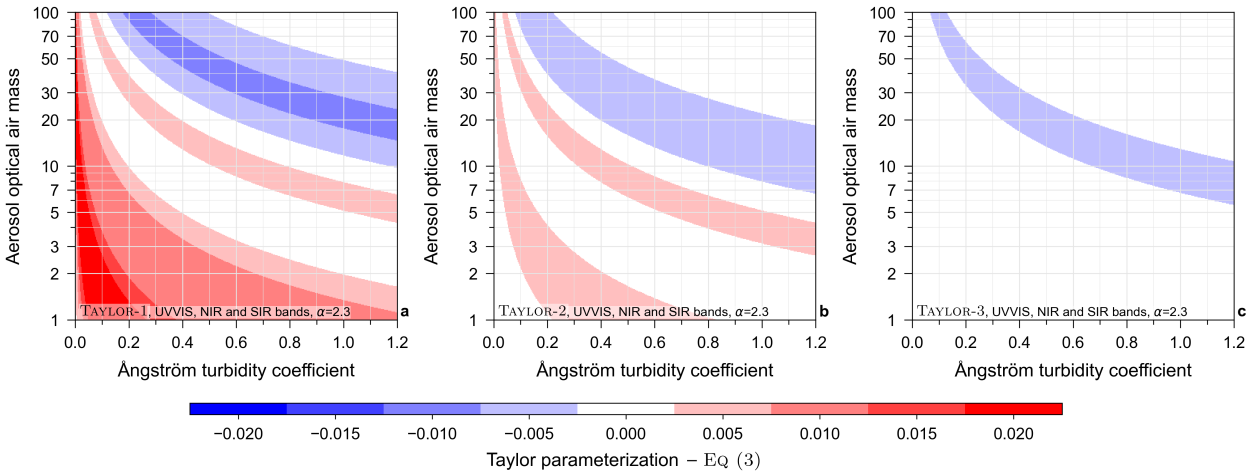

Figure 6: Same as Fig. 5 but in the (β, m_a) space. A fixed value $\alpha = 2.3$ is assumed.

values of α, here a fixed α value of 2.3 is assumed to ensure that the evaluation is conducted under the most challenging conditions. The deviations stay always smaller than 0.0075, in magnitude, for TAYLOR-2. Similarly, TAYLOR-3 deviations remain below 0.0025 for most of the space. Note that m_a runs from 1 to 100, thus encompassing solar zenith angles from zero to ≈89.4°.

4.3. Comparison with existing parameterizations

Having proved, in previous sections, the superiority of the TAYLOR-2 and TAYLOR-3 parameterizations used in combination with the three sub-band discretization of the solar spectral range, this section focuses on their comparative results against same-class existing broadband aerosol transmittance parameterizations. To that aim, the aerosol parameterizations from the MMAC, SIMv2 and SUNFLUX CSR models are selected, based on the results shown in Figs. 2 and 3. The evaluation in this section makes use of aerosol observations, as described below, in order to yield meaningful results.

Figure 7 shows the reference T_a (panel a) and its difference with respect to TAYLOR-2, TAYLOR-3, MMAC, SIMv2 and SUNFLUX in the (β, α) space for a fixed air mass value of 1.5 (Fig. 7b–f). In order to gauge the significance of the results and improve their interpretation, the joint probability distribution of β and α, as observed in the Aerosol Robotic Network [AERONET; 38] for $m_a \approx 1.5$, is shown as contour isolines going from reddish for the highest probability of occurrence to light bluish for the lowest probability of occurrence. The dataset, which comprises observations from 213 AERONET sites spanning the period from 2000 to 2018, has been previously used in Refs. [39, 40, 27], where the interested reader can find more details. As shown by the contour lines, aerosols mostly distribute throughout the narrow space region of β values smaller than 0.2 and α values in the range 0.5–2.0.

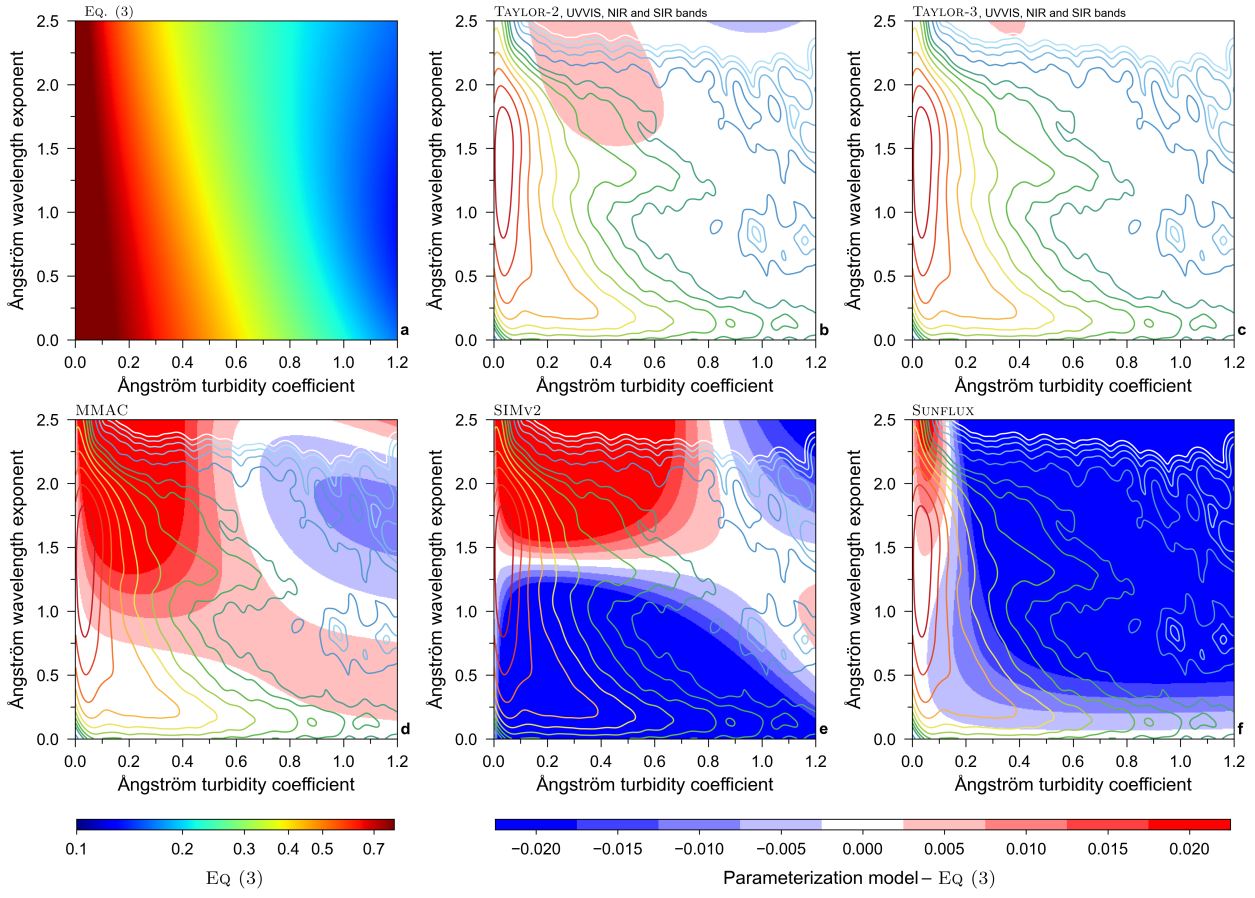

Figure 7: Reference T_a computed with Eq. (3) (panel a) and difference with respect to Taylor-2, Taylor-3, MMAC, SIMv2 and Sunflux (panels b-f) in the (β, α) space. The Taylor parameterization schemes are calculated over the UVVIS, NIR and SIR spectral bands. A fixed value $m_a = 1.5$ is assumed. The contour isolines display the joint probability distribution of β and α, going from reddish for the highest probability of occurrence to light bluish for the lowest probability of occurrence, as observed throughout 213 sites of the AERONET network during the 2000–2018 period for $m_a \approx 1.5$. A version of this figure (Fig. S1) that includes all models shown in Figs. 2 and 3 is provided in the supplementary material.

Figure 7 shows that the Taylor parameterization schemes perform much better than the existing ones, particularly, over the space region with the highest probability of aerosol occurrence. Interestingly, Taylor-3 provides deviations lower than 0.0025, in magnitude, virtually everywhere. MMAC shows greater deviations almost everywhere, especially in the region with α greater than about 1 and β smaller than about 0.4, where it overestimates the reference T_a. Contrarily, it has an outstanding performance for low α values, which suggests that it should produce quite good evaluations of aerosol transmittance at sites with prevailing coarse aerosols. SIMv2 neglects variations of α and the results suggest that the model probably assumes a fixed α value of ≈1.4. The absolute deviations with respect to the reference T_a grow sharply, and can reach or exceed 0.0175 when the value of α progressively deviates from 1.4 in either direction. Based on this result, it can be expected that this model produces biased results under desert or polluted

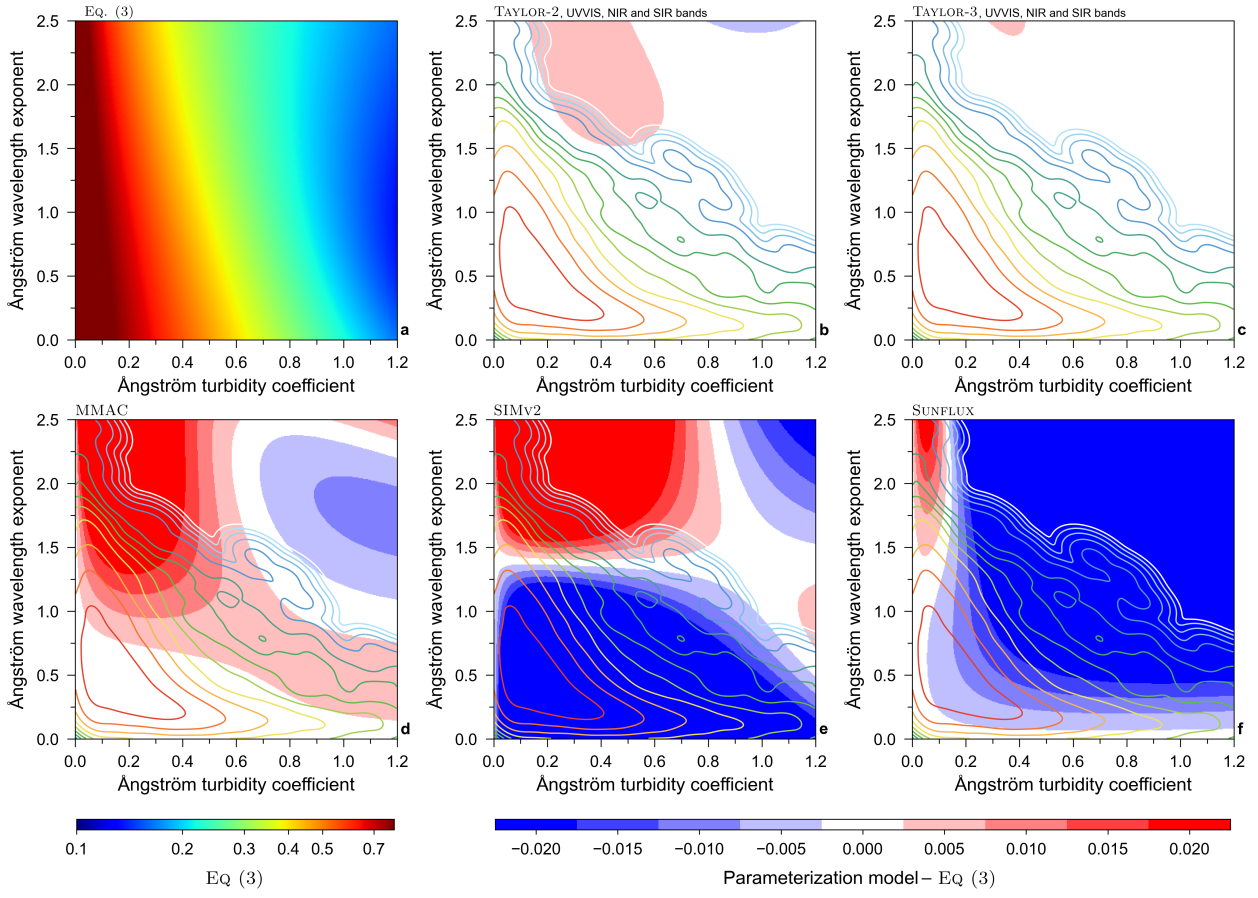

Figure 8: Same as Fig. 7, but with contour isolines for AERONET sites with prevailing coarse aerosols only. A version of this figure (Fig. S2) that includes all models shown in Figs. 2 and 3 is provided in the supplementary material.

conditions. SUNFLUX is characterized by large underestimations (≈0.02) for most of the (β, α) space. However, it results in low absolute deviations right in the space region with the highest probability of occurrence of aerosol. This is a symptom of model *overfitting*, which can produce quite good evaluations of broadband aerosol transmittance under average conditions while diverging under less frequent conditions because the parameterization does not properly generalize the true aerosol extinction process.

To further assess how the parameterization models behave under various aerosol conditions, the AERONET sites used to create the isolines in Fig. 7 are classified into prevailing coarse aerosol sites (those with prevailing dry desert conditions), mixed aerosol sites (those with rural or continental conditions) and fine aerosol sites (those with biomass burning or polluted urban conditions) using the clustering approach described in Ref. [39].

Figure 8 displays the contour isolines of the joint probability distribution of β and α for the sites with prevailing coarse aerosols. The aerosol's optical characteristics mostly distribute over the space region with β values up to ≈0.5 and α values below 1.3. In this case, the events with very large turbidity are characterized by low α values. Based on this

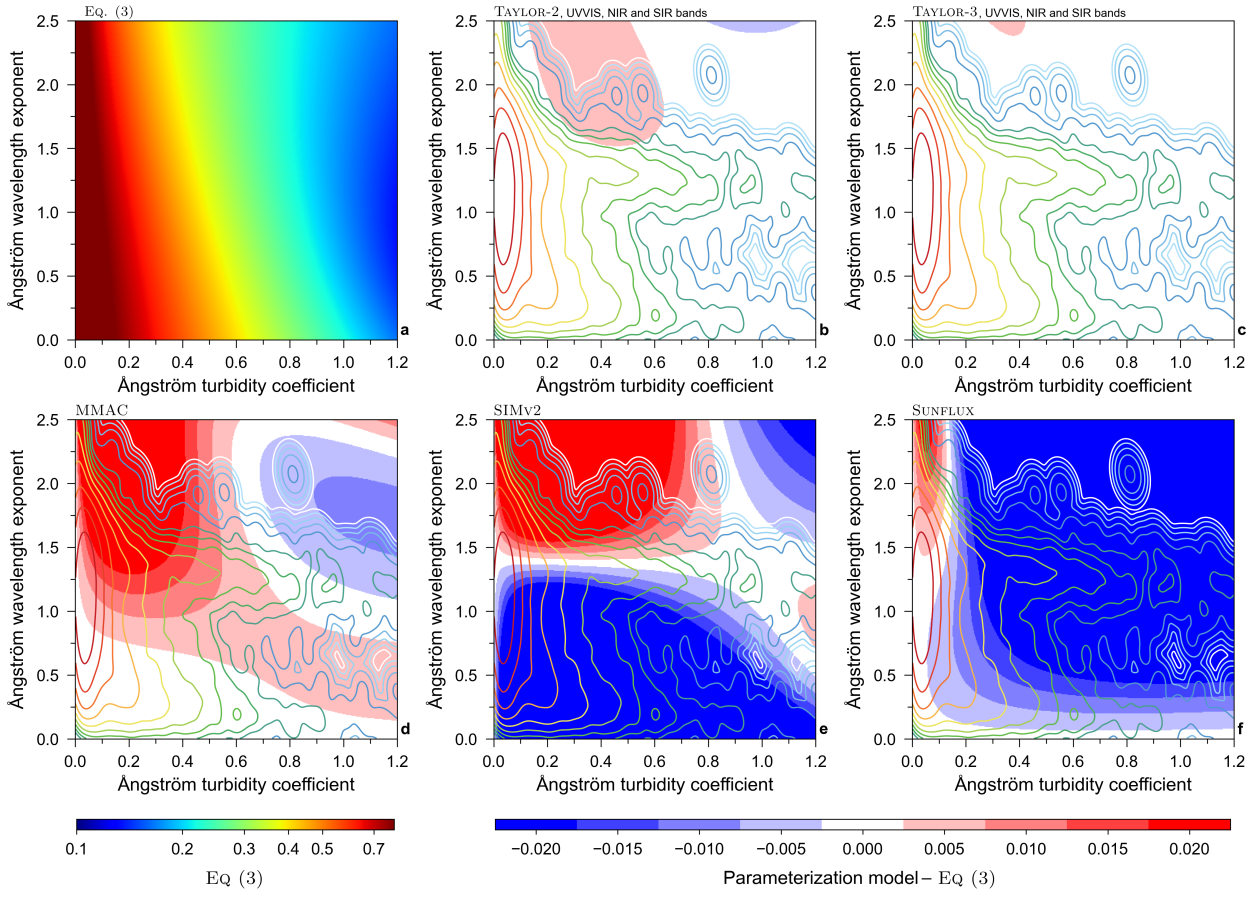

Figure 9: Same as Fig. 7, but with contour isolines for AERONET sites with prevailing mixed aerosols only. A version of this figure (Fig. S3) that includes all models shown in Figs. 2 and 3 is provided in the supplementary material.

data distribution, it is clear that Taylor-2 and Taylor-3 produce unbiased estimates of the reference T_a. In contrast, the reference T_a is strongly underestimated by SIMv2 and slightly underestimated by Sunflux, but well reproduced by MMAC. Figure 9 is similar to Fig. 8, but for sites with prevailing mixed aerosol type. The data distribution is very similar to that for all aerosols (Fig. 7) and, thus, the results are also alike. The case for prevailing fine-aerosol sites is shown in Fig. 10. There, the modal value of α increases. More specifically, high-turbidity events are characterized by a typical value of α between 1.5 and 2.0. Again, Taylor-2 and Taylor-3 reveal an outstanding performance at estimating the reference T_a, in contrast with the significant deviations that are expected with MMAC, SIMv2 and Sunflux. None of them correctly reproduces the results of Eq. (3) under these conditions.

The joint probability distribution of β and α can be used in combination with the broadband aerosol transmittances shown in Figs. 7–10 to estimate the global mean (noted as μ_ε or MB—mean bias), and standard deviation (noted as σ_ε or SD—standard deviation) of the differences between the reference T_a and the parameterization estimates, as follows:

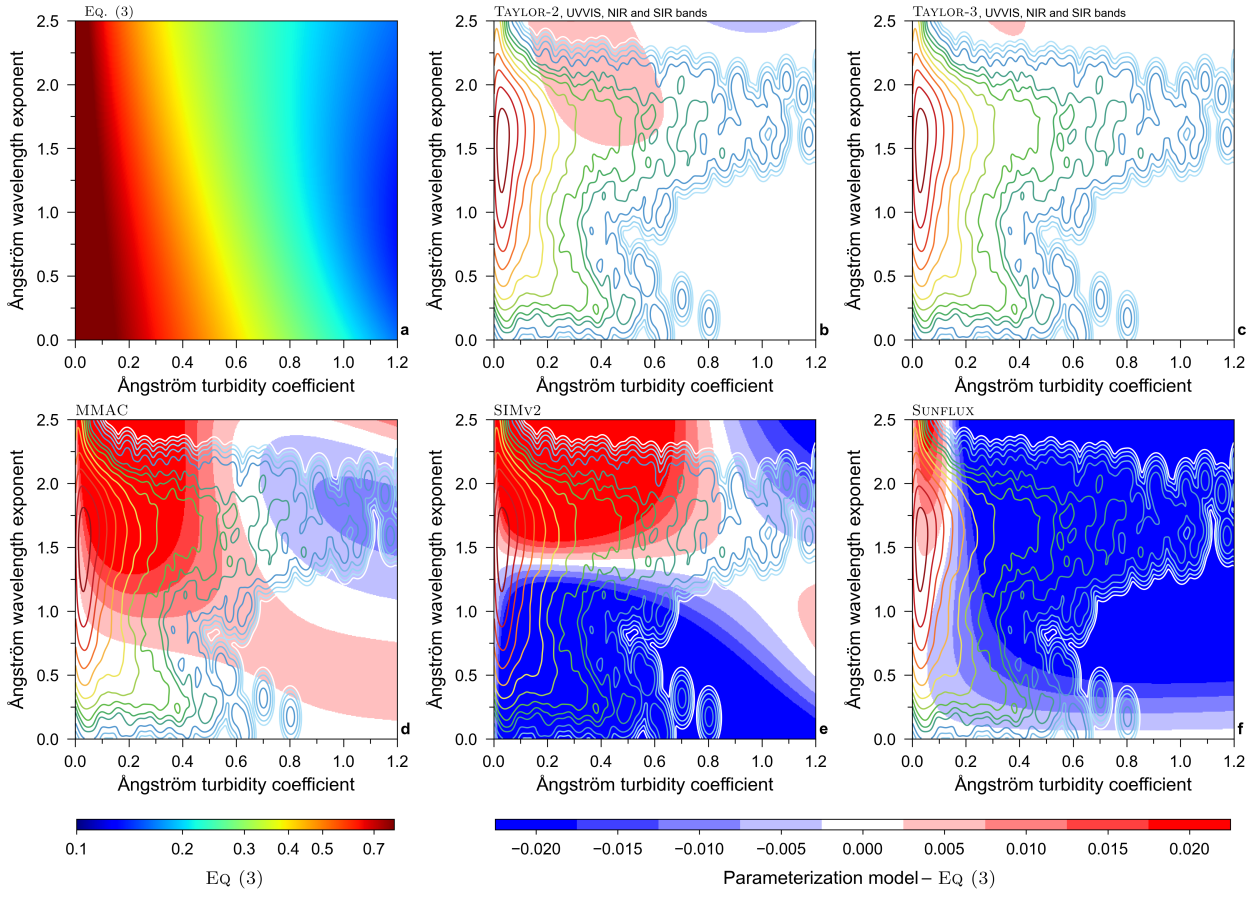

Figure 10: Same as Fig. 7, but with contour isolines for AERONET sites with prevailing fine aerosols only. A version of this figure (Fig. S4) that includes all models shown in Figs. 2 and 3 is provided in the supplementary material.

$$\mu_\varepsilon = \int \int \varepsilon(\beta, \alpha)\, P(\beta, \alpha)\, d\beta\, d\alpha, \tag{13}$$

$$\sigma_\varepsilon^2 = \int \int \left[\varepsilon(\beta, \alpha) - \mu_\varepsilon\right]^2\, P(\beta, \alpha)\, d\beta\, d\alpha, \tag{14}$$

where $\varepsilon(\beta, \alpha)$ represents the differences between the parameterization estimates and the reference T_a and $P(\beta, \alpha)$ is the joint probability distribution of β and α. Table 5 shows the MB and SD values for each parameterization scheme and aerosol type.

Overall, besides Taylor-2 and Taylor-3, only MMAC, Sunflux and CPCR2 yield MB and SD values smaller

Table 5
Mean bias (MD) and standard deviation (SD) of the differences between the reference T_a and the aerosol transmittance parameterizations described in Appendix A for each aerosol dataset. The values are calculated from the observed joint probability distributions of β and α as indicated by Eqs. (13) and (14). Values smaller than 0.01 are highlighted in bold face. The calculation for MRMv5 assumes sea-level pressure.

	All sites		Coarse aerosol		Mixed aerosol		Fine aerosol	
	MB	SD	MB	SD	MB	SD	MB	SD
TAYLOR-2	**0.001**	**0.000**	**0.000**	**0.000**	**0.001**	**0.000**	**0.001**	**0.001**
TAYLOR-3	**0.001**	**0.000**	**0.000**	**0.000**	**0.000**	**0.000**	**0.001**	**0.000**
MMAC	**0.008**	0.010	**0.001**	**0.004**	**0.006**	**0.007**	0.012	0.010
SIMv2	–0.016	0.038	–0.064	0.035	–0.018	0.029	**0.003**	0.023
SUNFLUX	**–0.001**	**0.008**	**–0.006**	**0.005**	**–0.002**	**0.008**	**0.001**	0.010
BIRD	–0.018	0.043	0.035	0.053	–0.017	0.031	–0.038	0.028
MIC	**0.004**	0.038	0.042	0.071	**–0.002**	0.025	**–0.005**	0.011
REST	–0.011	0.036	–0.057	0.034	–0.013	0.028	**0.008**	0.023
CPCR2	**0.000**	**0.008**	–0.010	0.012	**0.000**	**0.005**	**0.003**	**0.003**
MRMv5	–0.010	0.036	–0.055	0.034	–0.012	0.027	0.010	0.023

than 0.01 for any, or nearly any, aerosol type. However, compared to those three, the Taylor parameterizations yield much better results since they produce virtually unbiased estimates of the reference T_a with no dispersion regardless of aerosol type. The performance of the remaining models is inconsistent, and highly depends on aerosol type. For instance, the MB of SIMv2 for coarse aerosols is very high, in magnitude, (–0.064) despite being low for fine aerosols (0.003). It is also interesting to note that, surprisingly, the results obtained with REST and MRMv5 are virtually identical even though they are based on different parameterizations.

4.4. Computational burden

From an operational point of view, a critical feature of the parameterizations is their execution time. It must be the lowest possible with accuracy constrained within tolerable bounds. Otherwise, it would not make sense to use such parameterizations as a replacement for Eq. (3). Table 6 compares the execution times of the direct integration of Eq. (3) and the aerosol parameterizations described in Appendix A using the execution time of the aerosol transmittance parameterization in REST2v5 [16] as unit reference. That parameterization is not directly comparable to the ones evaluated here because it is based on a different paradigm of aerosol transmittance that cannot be represented by Eq. (3). However, it is a model that consistently performs high in comparative rankings [41, 12, 42, 3], so that its execution time is a fair reference here.

The results in Table 6 show that the parameterizations reduce the calculation time of aerosol transmittance by, at least, about 400 times with respect to the explicit integration of Eq. (3). Moreover, the increase of the parameterization accuracy is at the expense of computational time: TAYLOR-2 and TAYLOR-3, which are the most accurate according

to Table 5, are also the slowest. Nonetheless, their execution times are similar to that of REST2v5, which means that they are under tolerable bounds. Interestingly, MMAC has only half of the execution time of REST2v5 or the Taylor parameterizations and still retains a very good performance according to Table 5.

Overall, based on the results in Tables 5 and 6, it may be concluded that, to obtain high accuracy with a CSR model operated worldwide, a robust parameterization such as TAYLOR-2 or TAYLOR-3 is advantageous, at the expense of computational cost. However, if the model is to be run over a limited area under aerosols of a known nature, a simpler model such as MMAC or SIMv2 is faster and can provide good performance depending on the aerosol type involved.

Table 6
Execution time relative to that of the aerosol parameterization of REST2v5 (1 means equal execution time as REST2v5). The values are the average of 500 executions with 2000 random samples per execution.

Eq. (3)	TAYLOR-2	TAYLOR-3	MMAC	SIMv2	SUNFLUX	BIRD	MIC	REST	CPCR2	MRMv5
420	1.0	1.1	0.5	0.1	0.8	0.8	0.2	0.2	0.9	0.3

5. Improvement of existing CSR models

In the last decade, several works have benchmarked the performance of the most popular CSR models over worldwide locations *(i)* vis-à-vis ground observations [43, 41, 1, 44, 45, 42]; *(ii)* against rigorous physically-based reference models [12]; or *(iii)* using synthetic gridded datasets from atmospheric reanalyses to evaluate the inter-CSR model differences [2]. Additionally, Sun et al. [3, 11] have recently presented two ambitious benchmark studies including 75 global CSR models and 95 direct and diffuse CSR models, respectively, with the important aim of establishing a performance ranking of all models. To that effect, those studies used ground observations of irradiance as reference, while using atmospheric reanalysis data as model inputs. Consequently, the resulting rank is not actually that of the CSR models themselves but of their combination with the particular atmospheric reanalysis data used to describe the atmosphere. Beyond this key remark, model rankings are conveniently presented by solar radiation component and climate class.

This section demonstrates that DNI assessment with existing CSR models can be largely improved by simply replacing their treatment of aerosol transmittance with the Taylor parameterization described in Section 3. This improvement is achieved even though the consequential change in each model's aerosol parameterization may interfere with other parameterizations in it, as will be discussed later.

To show the improvement in DNI predictions when the Taylor aerosol parameterization is used, the MIC, MMAC, SIMv2 and SUNFLUX CSR model codes have been updated to include the TAYLOR-3 parameterization in such a

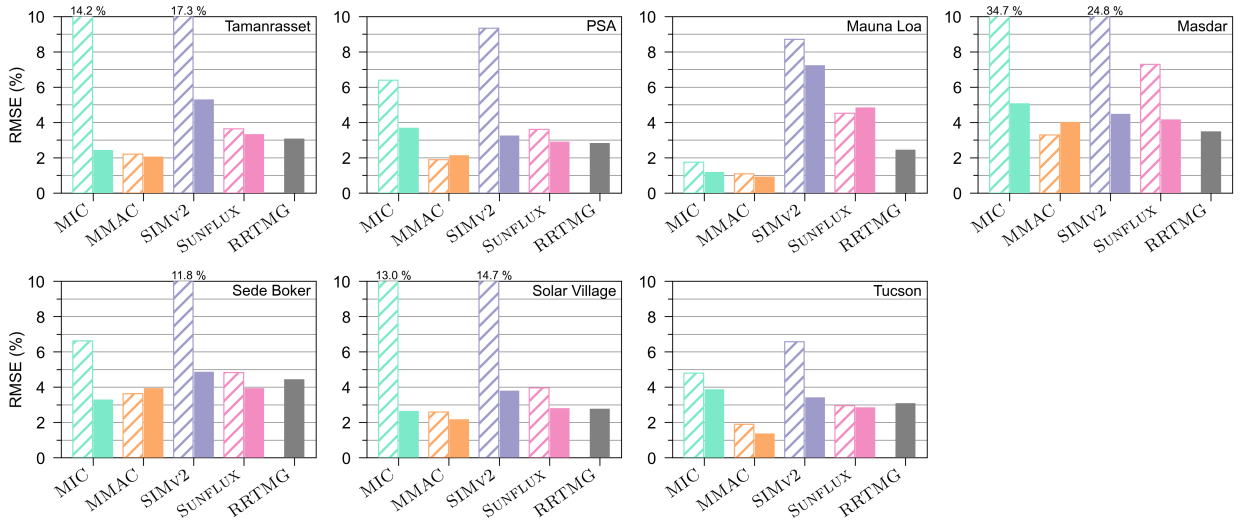

Figure 11: Root mean square error (RMSE) of the MIC, MMAC, SIMv2 and SUNFLUX models, with (full bars) and without (stripped bars) the TAYLOR-3 parameterization, at the 7 observational sites of the Gueymard and Ruiz-Arias [1] database. The RMSE of the physical RRTMG model provides a high-performance reference. When the RMSE of a model is greater than the maximum y-axis value, the actual RMSE value is annotated in the panel.

way that they can run with their original aerosol parameterization or with TAYLOR-3. The models' performance at predicting DNI is assessed from the observational database used in the benchmarking study of Gueymard and Ruiz-Arias [1] as a ground reference. It is made up of 7 observing sites at arid locations: Solar Village (Saudi Arabia), Tamanrasset (Algeria), Sede Boker (Israel), Mauna Loa (Hawaii), Masdar (Masdar Institute, Abu Dabhi), Plataforma Solar de Almería, hereafter PSA, (Spain) and Tucson (Arizona, USA). All sites feature 1-min observations of DNI collocated with observations of aerosol Ångström's parameters, β and α, and precipitable water from AERONET. Ozone and atmospheric pressure are also gathered from the AERONET data files. The interested reader may find a detailed description of the database in Ref. [1]. The cloud-screening process for this case study has been updated to the algorithm described in Ruiz-Arias et al. [46], causing slight difference in the results with respect to those in Ref. [1]. This recent cloud-screening algorithm is specifically designed to isolate those situations in which the sun's disc is not covered by any cloud as seen from the observer's vantage point, which means that clouds can still exist at other locations across the sky dome. This is sufficient for the case example conducted here because the verified variable is DNI.

Figure 11 compares the root mean square error (RMSE) of the selected CSR models—with and without the TAYLOR-3 parameterization—at the 7 observational sites, and also shows the results obtained with the high-performance physical and multiband RRTMG model [47, 48, 12], which is selected here as a reference because of its prominent status in meteorological and atmospheric applications. The Taylor parameterization improves the performance nearly

at all sites and for all models, with the only exceptions of SUNFLUX at Mauna Loa and MMAC at PSA, Masdar and Sede Boker, for which, in any case, the model degradation is small. When using their native aerosol transmittance functions, SUNFLUX and MMAC are the best performing CSR models, having results comparable to RRTMG. This explains that the Taylor parameterization does not always induce improvements with those two models. Nonetheless, its use still improves the results overall. For instance, the SUNFLUX RMSE at the haziest locations, Masdar and Solar Village, is reduced from 7 % to 4 % (i.e., by nearly 50 %) and from 4 % to less than 3 % (i.e., by ≈25 %), respectively.

On the other hand, the native MIC and SIMV2 models generally achieve very poor performance, which is worse at hazier locations. For instance, the RMSE at the Masdar site (the haziest location in this set of sites) is about 35 % and 25 % for MIC and SIMV2, respectively. Nonetheless, the use of the TAYLOR-3 parameterization is able to reduce the RMSE down to 5 % for MIC (i.e., a reduction of ≈85 %) and to 4.5 % for SIMV2 (i.e., a reduction of ≈75 %). These remarkable improvements diminish the RMSE of all models to values comparable to those of RRTMG at nearly all sites. The notable exception is Mauna Loa—a very particular site because of its high elevation above mean sea level (3397 m) and extremely low aerosol turbidity (annual mean β=0.008). It also proves the tremendous importance of aerosols in the evaluation of DNI with CSR models.

Notwithstanding, the overall improvement in DNI prediction when the TAYLOR-3 parameterization is used may lead to a deterioration of the same magnitude, or even greater, in the evaluation of the diffuse irradiance (DIF), and thus, foreseeably, in the global horizontal irradiance (GHI). For instance, Fig. 12 shows the scatterplots of observed vs. simulated DNI and GHI with the SIMV2 model at the Masdar and PSA locations. The results with the RRTMG model are also shown for reference. Whereas the improvement in DNI is substantial, the opposite occurs with GHI. This is apparently because the diffuse irradiance in this model, as with most similar models, is adjusted empirically to fit the estimates of a high-performance reference model, at least to some extent. The aerosol transmittance is an important part in such adjustment. Therefore, if the aerosol transmittance changes, the DIF component is impacted. As a consequence, the DIF component should be re-fitted considering the updated aerosol transmittance parameterization. This is just an example of how different partial biases interact in most current CSR models.

6. Conclusions

While presenting ambitious validation studies of clear-sky solar radiation models, recent contributions [3, 11] highlighted that many of them appeared to suffer from the consequences of over-fitting empirical relationships to training data, resulting in inconsistent worldwide performance. Here, a review of some of those models was conducted and unequivocally showed that most of the noted inconsistencies could be traced back to deficiencies in the parameterization of broadband aerosol extinction. This motivated the present study, considering that, in a global context, *(i)* aerosol

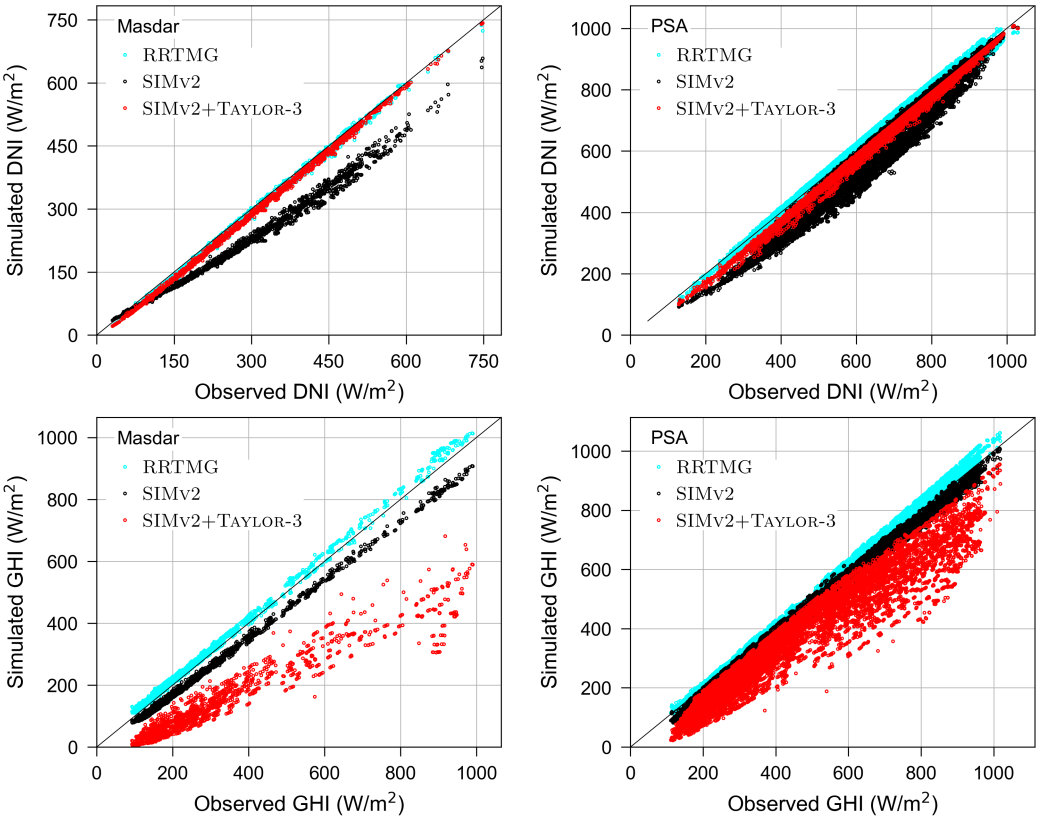

Figure 12: Observations *vs.* simulated DNI (upper row) and GHI (lower row) with the SIMv2 model at the Masdar (left) and PSA (right) locations. The simulated values with the RRTMG model are shown as a visual high-performance reference.

extinction is dominant in cloudless atmospheres; *(ii)* aerosols are subject to wide variations over both space and time; *(iii)* and the broadband solar irradiance extinction is also affected by spectral changes in their optical depth. So far, all the parameterizations of broadband aerosol transmittance have consisted in fitting a custom functional form to reference data, at least to some extent. This approach suffers from locality issues and lack of generality, hence existing clear-sky solar radiation (CSR) models rarely perform consistently under all aerosol conditions, ranging from coarse aerosols in dusty environments to fine aerosols in highly polluted atmospheres.

Here, a fast analytical aerosol transmittance parameterization has been presented. It has proven virtually unbiased and free of random deviations under all aerosol conditions with respect to the explicit integration of the spectral aerosol transmittance. It can be used universally as a surrogate for the native broadband aerosol transmittance in various widely-used CSR models to reduce their initial biases to the same level as that of the high-performance RRTMG physical model.

Specifically, the evaluation of DNI has been assessed by augmenting the MIC, MMAC, SIMv2 and Sunflux

CSR models with the new aerosol transmittance parameterization. The models were alternatively run with their native configuration and with the new parameterization, throughout a data base of 1-min DNI observations collocated with AERONET observations at 7 arid locations. The overall performance of all models improved with the new parameterization. In particular, the models with the poorest performance in this data base, namely, MIC and SIMv2, were improved by more than 75 % at the haziest locations. Overall, when the new aerosol parameterization was used, all the models performed similarly to the high-performance RRTMG physical model at nearly all locations. This fact proves that the accurate parameterization of aerosol transmittance in CSR models is an issue of the utmost importance. When aerosol transmittance is accurately parameterized, even the simplest CSR models yield DNI estimates comparable to those of high-performance (but comparatively slow) physical models.

Acknowledgments

The author thanks the personnel of the AERONET network who kindly acquired, processed and shared publicly the aerosol optical depth data used in this study, which have been retrieved from *https://aeronet.gsfc.nasa.gov*. The author thanks also the scientists and personnel of the BSRN network, Peter Armstrong of Masdar Institute, David Longenecker of NOAA, Stefan Wilbert of PSA-DLR and Lourdes Ramírez of CIEMAT for providing the solar irradiance data to validate the models. The author is also grateful to Dr. Christian A. Gueymard for sharing the Gueymard [34] solar irradiance spectrum, as well as for editing and improving the manuscript.

Supplementary data

Supplementary data to this article can be found online at `https:/doi.org/10.1016/j.rser.2021.111061`.

A. Existing aerosol transmittance parameterizations

In the description of the aerosol transmittance parameterizations that follows, the Ångström parameters β and α are used recurrently. The former, the turbidity coefficient, is AOD at 1 μm. The latter, the wavelength exponent, is most typically obtained based on the standard of the Aerosol Robotic Network [AERONET; 38], which considers a linear *log-log* fit of the AOD observations in the spectral channels between 440 nm and 870 nm (typically, 440, 500, 675 and 870 nm). For any solar zenith angle θ_z, the air mass (or aerosol optical mass, depending on model), m_a, is calculated with a model-specific formula.

The aerosol transmittance parameterizations are named after the hosting clear-sky solar radiation model in each case.

A.1. BIRD

The BIRD model [13] is a popular classical model, which parameterizes T_a from AOD at 380 nm, $\tau_{a,0.38}$, and at 500 nm, $\tau_{a,0.50}$, as follows:

$$T_a = \exp(-m_a^{0.9108}\ (1 + \tau_a - \tau_a^{0.7088})\ \tau_a^{0.873}) \tag{A.1a}$$

$$\tau_a = 0.2758\ \tau_{a,0.38} + 0.35\ \tau_{a,0.50} \tag{A.1b}$$

where $m_a = [\cos\theta_z + 0.15/(93.885 - \theta_z)^{1.25}]^{-1}$ and, for convenience, $\tau_{a,0.38}$ and $\tau_{a,0.50}$ are computed using the Ångström's law as $\tau_{a,0.38} = \beta\ 0.38^{-\alpha}$ and $\tau_{a,0.50} = \beta\ 0.50^{-\alpha}$.

A.2. MMAC

The modified MAC [MMAC; 30] model is also a well-known classical model that has ranked third for direct normal irradiance in a recent worldwide performance assessment of clear-sky solar radiation models [11].

The simplistic aerosol transmittance in the original MAC model [49, 50] was shown to degrade the model's performance significantly [51]. In consequence, Gueymard [30] suggested to use $T_a = \exp(-m'_a\tau_a)$ where τ_a is the Unsworth-Monteith broadband aerosol coefficient and m'_a is the pressure-corrected air mass.

Following Gueymard's suggestion, Sun et al. [11] have evaluated the combination of MMAC with different parameterizations of τ_a. They found that Eq. (32) of Ref. [43] resulted in the best direct normal irradiance performance. Hence, that aerosol transmittance parameterization is evaluated here:

$$T_a = \exp(-m_a\ \tau_a) \tag{A.2a}$$

$$\tau_a = \beta\ \lambda_e^{-\alpha} \tag{A.2b}$$

$$\lambda_e = 0.695 + m_a\ (0.016 + 0.066\ \beta\ 0.7^{-\alpha}) \tag{A.2c}$$

where $m_a = 35/(1 + 1224\ \cos^2\theta_z)^{0.5}$. Note that the air mass in the parameterization considered here is not pressure corrected.

A.3. MIC

Gueymard [43] proposed the replacement of the broadband aerosol transmittance in the Iqbal's parameterization model C by that of the Iqbal's parameterization model A—both models were originally proposed by Iqbal [52]—and named the resultant model *modified Iqbal-C* (here, referred to as MIC). It parameterizes the aerosol transmittance from

α and β as follows:

$$T_a = 0.12445\ \alpha - 0.0162 + (1.003 - 0.125\ \alpha)\ \exp[-\beta\ m_a\ (1.089\ \alpha + 0.5123)], \tag{A.3}$$

where $\beta < 0.5$ and m_a is computed as in the BIRD model.

A.4. CPCR2

The Code for Physical Computation of Radiation, 2 bands, [CPCR2; 14] is a pioneering two-band clear-sky solar irradiance model with the separation of spectral bands at 700 nm. The aerosol transmittance parameterization relies on α and β, and is parameterized as follows:

$$T_a = 0.4708\ T_{a1} + 0.5292\ T_{a2} \tag{A.4a}$$

$$T_{ai} = \exp(-m_a\ \beta\ \lambda_{ei}^{-\alpha}), \quad i = 1, 2 \tag{A.4b}$$

$$\lambda_{ei} = a_{i0} + a_{i1}\ u_a + a_{i2}\ u_a^2, \quad i = 1, 2 \tag{A.4c}$$

$$u_a = \ln(1 + m_a\ \beta) \tag{A.4d}$$

$$a_{10} = 0.510941 - 0.028607\ \alpha + 0.006835\ \alpha^2 \tag{A.4e}$$

$$a_{11} = -0.026895 + 0.054857\ \alpha + 0.006872\ \alpha^2 \tag{A.4f}$$

$$a_{12} = 0.009649 + 0.005536\ \alpha - 0.009349\ \alpha^2 \tag{A.4g}$$

$$a_{20} = 1.128036 - 0.0642\ \alpha + 0.005276\ \alpha^2 \tag{A.4h}$$

$$a_{21} = -0.032851 + 0.036112\ \alpha + 0.005066\ \alpha^2 \tag{A.4i}$$

$$a_{22} = 0.027787 + 0.064655 - 0.021385\ \alpha^2 \tag{A.4j}$$

where $0.05 < m_a\ \beta < 8$, $0.5 < \alpha < 2.5$ and $m_a = [\cos(\theta_z) + 0.0548/(92.65 - \theta_z)^{1.452}]^{-1}$. The original formulation was devised for separate α values in each band, but the model's author suggested also the use of the same α value in the two bands. This is the approach that is adopted here. Moreover, the original band weighting factors of the model were derived from an extraterrestrial solar spectrum that is now outdated. Hence, the fractions obtained for the UVVIS and IR bands from the Gueymard [34] spectrum (see Table 2) are preferred, and thus they are used in Eq. (A.4a) to evaluate T_a. Note that the new weight for the IR band considers the spectral interval from 700 nm to 4000 nm, while the original formulation considered the interval from 700 nm to only 2700 nm.

A.5. REST

The Reference Evaluation of Solar Transmittance (REST) model is a broadband model fully described in Ref. [30] and a precursor of the well-known REST2 model [16]. REST parameterizes the aerosol transmittance as follows:

$$T_a = \exp(-m_a\ \tau_a) \tag{A.5a}$$

$$\tau_a = \beta\ \frac{e_0 + e_1\ m_a}{1 + e_2\ m_a} \tag{A.5b}$$

$$e_0 = 1.6933 \tag{A.5c}$$

$$e_1 = \frac{-0.013029 + 0.13126\ \beta}{1 + 0.42003\ \beta} \tag{A.5d}$$

$$e_2 = \frac{-0.0083581 + 0.40323\ \beta + 0.123\ \beta^2}{1 + 0.42003\ \beta} \tag{A.5e}$$

where $m_a = [\cos\theta_z + 0.16851\ \theta_z^{0.18198}/(95.318 - \theta_z)^{1.9542}]^{-1}$.

A.6. MRMv5

The all-sky Meteorological Radiation Model, version 5, [MRMv5; 53] is a revised version from previous model releases where various errors were corrected. The aerosol transmittance parameterization is borrowed from Refs. [54, 55]:

$$T_a = \exp(-m_a\ \tau_a) \tag{A.6a}$$

$$\tau_a = \beta\ \lambda_e^{-1.3} \tag{A.6b}$$

$$\lambda_e = 0.6777 + 0.1464\ u_a - 0.00626\ u_a^2 \tag{A.6c}$$

where $u_a = m_a\ \beta$ and $m_a = \left(\frac{p}{p_o}\right)[\cos(\theta_z) + 0.50572/(96.07995 - \theta_z)^{1.6364}]^{-1}$, where p and p_o are the site and sea-level atmospheric pressure, respectively. In this work, MRMv5 is run for sea-level atmospheric pressure conditions (*i.e.*, $p = p_o$).

The aerosol transmittance calculation in the current version of the model (v6) has evolved [32], and T_a is now computed from a spectral integral that is similar to Eq. (3) above.

A.7. SIMv2

The Solar Irradiance Model, version 2 [56], is a recent overhaul of a previous version [57]. SIMv2 uses β (but not α) to parameterize the aerosol transmittance as follows:

$$T_a = \frac{1 - 0.046\,u_a}{1 + 1.73849\,u_a + 0.79081\,u_a^2}, \tag{A.7}$$

where $u_a = m_a\beta$ and $m_a = [\cos\theta_z + 0.031141\ \theta_z^{0.1}/(92.471 - \theta_z)^{1.3814}]^{-1}$.

A.8. SUNFLUX

The SUNFLUX model has been described in a suite of publications [19, 36, 18]. It is a two-band model that simulates both cloudless and cloudy situations. Just recently, the authors of the model have published a new parameterization of the aerosol transmittance, which is the one used here [58]:

$$T_a = 0.45389\ T_{a1} + 0.54611\ T_{a2} \tag{A.8a}$$

$$T_{a1} = \exp(-m_{a1}\ \tau_{a,0.55}) \tag{A.8b}$$

$$m_{a1} = 1.00016/(\cos\theta_z)^{0.998945} \tag{A.8c}$$

$$T_{a2} = \exp(-m_{a2}\ \tau_{a,0.87}) \tag{A.8d}$$

$$m_{a2} = 1.00028/(\cos\theta_z)^{0.999166} \tag{A.8e}$$

where, for convenience, $\tau_{a,0.55} = \beta\ 0.55^{-\alpha}$ and $\tau_{a,0.87} = \beta\ 0.87^{-\alpha}$.

B. Derivation of the new aerosol transmittance parameterization

The Taylor expansion series of $T_{a\lambda}(\lambda)$ around the central wavelength, $\bar{\lambda}$, in a spectral band bounded by wavelengths λ_1 and λ_2 is:

$$T_{a\lambda}(\lambda) = T_{a\lambda}(\bar{\lambda}) + \sum_{n=1}^{\infty} \frac{1}{n!} \frac{d^n T_{a\lambda}}{d\lambda^n}\bigg|_{\bar{\lambda}} (\lambda - \bar{\lambda})^n, \tag{B.1}$$

where $T_{a\lambda}(\lambda)$ is given by Eq. (4). Inserting the Taylor expansion in Eq. (3) and considering that

$$P(\lambda) = \frac{E_{0n\lambda}(\lambda)}{\int_{\lambda_1}^{\lambda_2} E_{0n\lambda}(\lambda)}\, d\lambda, \tag{B.2}$$

subject to $\lambda_1 \leq \lambda \leq \lambda_2$, is the extraterrestrial solar irradiance probability distribution function throughout the spectral band bounded by λ_1 and λ_2, Eq. (3) results in:

$$T_a = T_{a\lambda}(\bar{\lambda}) \left[1 + \sum_{n=1}^{\infty} \frac{\bar{\lambda}^n}{T_{a\bar{\lambda}}} \frac{d^n T_{a\lambda}}{d\lambda^n}\bigg|_{\bar{\lambda}} I_n \right], \tag{B.3}$$

where

$$I_n = \frac{1}{n!} \int_{\lambda_1}^{\lambda_2} \left(\frac{\lambda}{\bar{\lambda}} - 1 \right)^n P(\lambda)\, d\lambda \tag{B.4}$$

are coefficients that *only* depend on the waveband choice and not on the atmospheric turbidity or sun's position. They are only related to the central moments of $P(\lambda)$.

Performing the derivatives of $T_{a\lambda}(\lambda)$ and defining $\phi = m\,\alpha\,\tau_{a\lambda}(\bar{\lambda})$, the first three derivatives are:

$$\frac{\bar{\lambda}}{T_{a\bar{\lambda}}} \frac{dT_{a\lambda}}{d\lambda}\bigg|_{\bar{\lambda}} = \phi \tag{B.5a}$$

$$\frac{\bar{\lambda}^2}{T_{a\bar{\lambda}}} \frac{d^2T_{a\lambda}}{d\lambda^2}\bigg|_{\bar{\lambda}} = \left[\frac{\bar{\lambda}}{T_{a\bar{\lambda}}} \frac{dT_{a\lambda}}{d\lambda}\bigg|_{\bar{\lambda}} - (\alpha+1) \right] \phi \tag{B.5b}$$

$$\frac{\bar{\lambda}^3}{T_{a\bar{\lambda}}} \frac{d^3T_{a\lambda}}{d\lambda^3}\bigg|_{\bar{\lambda}} = \left[\frac{\bar{\lambda}^2}{T_{a\bar{\lambda}}} \frac{d^2T_{a\lambda}}{d\lambda^2}\bigg|_{\bar{\lambda}} - 2(\alpha+1) \frac{\bar{\lambda}}{T_{a\bar{\lambda}}} \frac{dT_{a\lambda}}{d\lambda}\bigg|_{\bar{\lambda}} + (\alpha+1)(\alpha+2) \right] \phi. \tag{B.5c}$$

Defining $P_n(\phi) = \frac{\bar{\lambda}^n}{T_{a\bar{\lambda}}} \frac{d^n T_{a\lambda}}{d\lambda^n}\Big|_{\bar{\lambda}}$ and calculating higher-order derivatives, the polynomials defined by Eqs. (8-9) are found.

CRediT authorship contribution statement

José A. Ruiz-Arias: Conceptualization, Methodology, Data processing, Writing.

References

[1] C. A. Gueymard, J. A. Ruiz-Arias, Validation of direct normal irradiance predictions under arid conditions: A review of radiative models and their turbidity-dependent performance, Renew. Sust. Energ. Rev. 45 (2015) 379–396. doi:10.1016/j.rser.2015.01.065.

[2] J. A. Ruiz-Arias, C. A. Gueymard, Worldwide inter-comparison of clear-sky solar radiation models: Consensus-based review of direct and global irradiance components simulated at the earth surface, Sol. Energy 168 (2018) 10–29. doi:10.1016/j.solener.2018.02.008.

[3] X. Sun, J. M. Bright, C. A. Gueymard, B. Acord, P. Wang, N. A. Engerer, Worldwide performance assessment of 75 global clear-sky irradiance models using Principal Component Analysis, Renew. Sust. Energ. Rev. 111 (2019) 550–570. doi:10.1016/j.rser.2019.04.006.

[4] C. A. Gueymard, Clear-Sky Radiation Models and Aerosol Effects, in: J. Polo, L. Martín-Pomares, A. Sanfilippo (Eds.), Solar Resources Mapping, Springer International Publishing, 2019, pp. 137–182. doi:10.1007/978-3-319-97484-2{_}5.

[5] R. Perez, T. Cebecauer, M. Šúri, Semi-empirical satellite models, in: J. Kleissl (Ed.), Solar Energy Forecasting and Resource Assessment, Elsevier, 2013, pp. 21–48. doi:10.1016/B978-0-12-397177-7.00002-4.

[6] N. Engerer, F. Mills, Kpv: A clear-sky index for photovoltaics, Sol. Energy 105 (2014) 679–693. doi:10.1016/j.solener.2014.04.019.

[7] C. A. Gueymard, J. M. Bright, D. Lingfors, A. Habte, M. Sengupta, A posteriori clear-sky identification methods in solar irradiance time series: Review and preliminary validation using sky imagers, Renew. Sust. Energ. Rev. 109 (2019) 412–427. doi:10.1016/j.rser.2019.04.027.

[8] J. Bright, C. Smith, P. Taylor, R. Crook, Stochastic generation of synthetic minutely irradiance time series derived from mean hourly weather observation data, Sol. Energy 115 (2015) 229–242. doi:10.1016/j.solener.2015.02.032.

[9] C. E. Duchon, M. S. O'Malley, Estimating cloud type from pyranometer observations, J. Appl. Meteorol. 38 (1999) 132–141. doi:10.1175/1520-0450(1999)038<0132:ECTFPO>2.0.CO;2.

[10] C. A. Gueymard, J. A. Ruiz-Arias, Extensive worldwide validation and climate sensitivity analysis of direct irradiance predictions from 1-min global irradiance, Sol. Energy 128 (2016) 1–30. doi:10.1016/j.solener.2015.10.010.

[11] X. Sun, J. M. Bright, C. A. Gueymard, X. Bai, B. Acord, P. Wang, Worldwide performance assessment of 95 direct and diffuse clear-sky irradiance models using principal component analysis, Renew. Sust. Energ. Rev. 135 (2021) 110087. doi:10.1016/j.rser.2020.110087.

[12] J. A. Ruiz-Arias, C. A. Gueymard, A multi-model benchmarking of direct and global clear-sky solar irradiance predictions at arid sites using a reference physical radiative transfer model, Sol. Energy 171 (2018) 447–465. doi:10.1016/j.solener.2018.06.048.

[13] R. E. Bird, R. L. Hulstrom, Simplified clear sky model for direct and diffuse insolation on horizontal surfaces, Technical Report SERI/TR/642-761, Solar Energy Research Institude, Golden, CO, 1981. doi:10.2172/6510849.

[14] C. A. Gueymard, A two-band model for the calculation of clear sky solar irradiance, illuminance, and photosynthetically active radiation at the Earth's surface, Sol. Energy 43 (1989) 253–265. doi:10.1016/0038-092X(89)90113-8.

[15] C. Rigollier, O. Bauer, L. Wald, On the clear sky model of the ESRA – European Solar Radiation Atlas – with respect to the Heliosat method, Sol. Energy 68 (2000) 33–48. doi:10.1016/s0038-092x(99)00055-9.

[16] C. A. Gueymard, REST2: High-performance solar radiation model for cloudless-sky irradiance, illuminance, and photosynthetically active radiation – Validation with a benchmark dataset, Sol. Energy 82 (2008) 272–285. doi:10.1016/j.solener.2007.04.008.

[17] P. Ineichen, A broadband simplified version of the Solis clear sky model, Solar Energy 82 (2008) 758–762. doi:10.1016/j.solener.2008.02.009.

[18] Z. Sun, X. Zeng, J. Liu, H. Liang, J. Li, Parameterization of instantaneous global horizontal irradiance: clear-sky component, Q. J. R. Meteorol. Soc. 140 (2014) 267–280. doi:10.1002/qj.2126.

[19] Z. Sun, J. Liu, X. Zeng, H. Liang, Parameterization of instantaneous global horizontal irradiance: Cloudy-sky component: Parameterization of global irradiance, J. Geophys. Res.-Atmos. 117 (2012). doi:10.1029/2012JD017557.

[20] J. Qin, W. Tang, K. Yang, N. Lu, X. Niu, S. Liang, An efficient physically based parameterization to derive surface solar irradiance based on satellite atmospheric products, J. Geophys. Res.-Atmos. 120 (2015) 4975–4988. doi:10.1002/2015JD023097.

[21] Y. Xie, M. Sengupta, J. Dudhia, A Fast All-sky Radiation Model for Solar applications (FARMS): Algorithm and performance evaluation, Sol. Energy 135 (2016) 435–445. doi:10.1016/j.solener.2016.06.003.

[22] H. Kambezidis, B. Psiloglou, D. Karagiannis, U. Dumka, D. Kaskaoutis, Meteorological Radiation Model (MRM v6.1): Improvements in diffuse radiation estimates and a new approach for implementation of cloud products, Renew. Sust. Energ. Rev. 74 (2017) 616–637. doi:10.1016/j.rser.2017.02.058.

[23] H. C. van de Hulst, Light scattering by small particles, Dover Publications, New York, 1981.

[24] B. Molineaux, P. Ineichen, On the broad band transmittance of direct irradiance in a cloudless sky and its application to the parameterization of atmospheric turbidity, Sol. Energy 56 (1996) 553–563. doi:10.1016/0038-092X(96)00016-3.

[25] C. A. Gueymard, Turbidity determination from broadband irradiance measurements: A detailed multicoefficient approach, J. Appl. Meteorol. 37 (1998) 414–435. doi:10.1175/1520-0450(1998)037<0414:TDFBIM>2.0.CO;2.

[26] J. A. Ruiz-Arias, C. A. Gueymard, Solar resource for high-concentrator photovoltaic applications, in: P. Pérez-Higueras, E. F. Fernández (Eds.), High Concentrator Photovoltaics: Fundamentals, Engineering and Power Plants, 2015, pp. 261–302. doi:doi:10.1007/978-3-319-15039-0_10.

[27] J. A. Ruiz-Arias, Bias in modeled solar radiation by non-resolved intra-daily AOD variability, Sol. Energy 205 (2020) 221–229. doi:10.1016/j.solener.2020.04.082.

[28] J. A. Ruiz-Arias, C. A. Gueymard, F. J. Santos-Alamillos, D. Pozo-Vázquez, Do spaceborne aerosol observations limit the accuracy of modeled surface solar irradiance?: Aerosol limits modeled solar radiation, Geophys. Res. Lett. 42 (2015) 605–612. doi:10.1002/2014GL062309.

[29] C. F. Bohren, E. E. Clothiaux, Fundamentals of Atmospheric Radiation: An Introduction with 400 Problems, Wiley–CH, Weinheim, Germany, 2006.

[30] C. A. Gueymard, Direct solar transmittance and irradiance predictions with broadband models. Part I: detailed theoretical performance assessment, Sol. Energy 74 (2003) 355–379. doi:10.1016/S0038-092X(03)00195-6.

[31] A. Ångström, On the atmospheric transmission of sun radiation and on dust in the air, Geogr. Ann. 11 (1929) 156–166. doi:10.2307/519399.

[32] H. Kambezidis, B. Psiloglou, D. Karagiannis, U. Dumka, D. Kaskaoutis, Recent improvements of the Meteorological Radiation Model for solar irradiance estimates under all-sky conditions, Renew. Energ. 93 (2016) 142–158. doi:10.1016/j.renene.2016.02.060.

[33] J. Polo, R. Perez, Solar radiation modeling from satellite imagery, in: J. Polo, L. Martín-Pomares, A. Sanfilippo (Eds.), Solar Resources Mapping: Fundamentals and Applications, Springer, 2019, pp. 183–197. doi:10.1007/978-3-319-97484-2_6.

[34] C. A. Gueymard, Revised composite extraterrestrial spectrum based on recent solar irradiance observations, Sol. Energy 169 (2018) 434–440. doi:10.1016/j.solener.2018.04.067.

[35] S. Clough, M. Shephard, E. Mlawer, J. Delamere, M. Iacono, K. Cady-Pereira, S. Boukabara, P. Brown, Atmospheric radiative transfer modeling: a summary of the AER codes, J. Quant. Spectrosc. Ra. 91 (2005) 233–244. doi:10.1016/j.jqsrt.2004.05.058.

[36] Z. Sun, A. Liu, Fast scheme for estimation of instantaneous direct solar irradiance at the Earth's surface, Sol. Energy 98 (2013) 125–137. doi:10.1016/j.solener.2012.12.013.

[37] T. A. Beu, Introduction to Numerical Programming. A Pratical Guide for Scientists and Engineers Using Python and C/C++, CRC Press, Taylor and Francis Group, Boca Raton, FL, USA, 2015.

[38] D. M. Giles, A. Sinyuk, M. G. Sorokin, J. S. Schafer, A. Smirnov, I. Slutsker, T. F. Eck, B. N. Holben, J. R. Lewis, J. R. Campbell, et al., Advancements in the Aerosol Robotic Network (AERONET) Version 3 database–automated near-real-time quality control algorithm with improved cloud screening for Sun photometer aerosol optical depth (AOD) measurements, Atmos. Meas. Tech. 12 (2019) 169–209. doi:10.5194/amt-12-169-2019.

[39] J. A. Ruiz-Arias, C. A. Gueymard, S. Quesada-Ruiz, F. J. Santos-Alamillos, D. Pozo-Vázquez, Bias induced by the AOD representation time scale in long-term solar radiation calculations. Part 1: Sensitivity of the AOD distribution to the representation time scale, Sol. Energy 137 (2016) 608–620. doi:10.1016/j.solener.2016.06.026.

[40] J. A. Ruiz-Arias, C. A. Gueymard, F. J. Santos-Alamillos, S. Quesada-Ruiz, D. Pozo-Vázquez, Bias induced by the AOD representation time scale in long-term solar radiation calculations. Part 2: Impact on long-term solar irradiance predictions, Sol. Energy 135 (2016) 625–632.

doi:10.1016/j.solener.2016.06.017.

[41] V. Badescu, C. A. Gueymard, S. Cheval, C. Oprea, M. Baciu, A. Dumitrescu, F. Iacobescu, I. Milos, C. Rada, Computing global and diffuse solar hourly irradiation on clear sky. Review and testing of 54 models, Renew. Sust. Energ. Rev. 16 (2012) 1636–1656. doi:10.1016/j.rser.2011.12.010.

[42] F. Antonanzas-Torres, R. Urraca, J. Polo, O. Perpiñán Lamigueiro, R. Escobar, Clear sky solar irradiance models: A review of seventy models, Renew. Sust. Energ. Rev. 107 (2019) 374–387. doi:10.1016/j.rser.2019.02.032.

[43] C. A. Gueymard, Clear-sky irradiance predictions for solar resource mapping and large-scale applications: Improved validation methodology and detailed performance analysis of 18 broadband radiative models, Sol. Energy 86 (2012) 2145–2169. doi:10.1016/j.solener.2011.11.011.

[44] N. Engerer, F. Mills, Validating nine clear sky radiation models in Australia, Sol. Energy 120 (2015) 9–24. doi:10.1016/j.solener.2015.06.044.

[45] P. Ineichen, Validation of models that estimate the clear sky global and beam solar irradiance, Sol. Energy 132 (2016) 332–344. doi:10.1016/j.solener.2016.03.017.

[46] J. A. Ruiz-Arias, C. A. Gueymard, T. Cebecauer, Direct normal irradiance modeling: Evaluating the impact on accuracy of worldwide gridded aerosol databases, AIP Conference Proceedings 2126 (2019) 190013. doi:10.1063/1.5117710.

[47] M. Iacono, J. Delamere, E. Mlawer, S. Clough, J.-J. Morcrette, Y.-T. Hou, Development and Evaluation of RRTMG_SW, a Shortwave Radiative Transfer Model for General Circulation Model Applications, in: Fourteenth ARM Science Team Meeting Proceedings, 2004, pp. 1–10. URL: https://www.arm.gov/publications/proceedings/conf14/extended_abs/iacono-mj.pdf.

[48] M. J. Iacono, J. S. Delamere, E. J. Mlawer, M. W. Shephard, S. A. Clough, W. D. Collins, Radiative forcing by long-lived greenhouse gases: Calculations with the AER radiative transfer models, J. Geophys. Res.-Atmos. 113 (2008) D13103. doi:10.1029/2008JD009944.

[49] J. A. Davies, W. Schertzer, M. Nunez, Estimating global solar radiation, Bound.-Lay. Meteorol. 9 (1975) 33–52. doi:10.1007/BF00232252.

[50] J. Davies, D. McKay, Evaluation of selected models for estimating solar radiation on horizontal surfaces, Sol. Energy 43 (1989) 153–168. doi:10.1016/0038-092X(89)90027-3.

[51] C. A. Gueymard, Critical analysis and performance assessment of clear sky solar irradiance models using theoretical and measured data, Sol. Energy 51 (1993) 121–138. doi:10.1016/0038-092X(93)90074-X.

[52] M. Iqbal, An introduction to solar radiation, Academic Press, New York, United States, 1983.

[53] H. D. Kambezidis, B. E. Psiloglou, The Meteorological Radiation Model (MRM): Advancements and Applications, in: V. Badescu (Ed.), Modeling Solar Radiation at the Earth's Surface: Recent Advances, Springer, Berlin, Heidelberg, 2008, pp. 357–392. doi:{10.1007/978-3-540-77455-6-14}.

[54] K. Yang, G. Huang, N. Tamai, A hybrid model for estimating global solar radiation, Sol. Energy 70 (2001) 13–22. doi:10.1016/S0038-092X(00)00121-3.

[55] K. Yang, T. Koike, B. Ye, Improving estimation of hourly, daily, and monthly solar radiation by importing global data sets, Agricultural and Forest Meteorology 137 (2006) 43–55. doi:10.1016/j.agrformet.2006.02.001.

[56] D. Calinoiu, N. Stefu, R. Boata, R. Blaga, N. Pop, E. Paulescu, A. Sabadus, M. Paulescu, Parametric modeling: A simple and versatile route to solar irradiance, Energ. Convers. Manage. 164 (2018) 175–187. doi:10.1016/j.enconman.2018.02.077.

[57] D. Calinoiu, M. Paulescu, I. Ionel, N. Stefu, N. Pop, R. Boata, A. Pacurar, P. Gravila, E. Paulescu, G. Trif-Tordai, Influence of aerosols pollution on the amount of collectable solar energy, Energ. Convers. Manage. 70 (2013) 76–82. doi:10.1016/j.enconman.2013.02.012.

[58] G. Shi, Z. Sun, J. Li, Y. He, Fast scheme for determination of direct normal irradiance. Part I: New aerosol parameterization and performance assessment, Sol. Energy 199 (2020) 268–277. doi:10.1016/j.solener.2020.02.028.